Constraining the pattern and magnitude of forced precipitation change in CMIP6

Maximilian Kotz[a b], Stefan Lange [a], Leonie Wenz [a c], Anders Levermann [a b d]

[a] *Potsdam Institute for Climate Impact Research*

[b] *Innstitute of Physics, University of Potsdam*

[c] *Mercator Research Institute on Global Commons and Climate Change*

[d] *Lamont-Doherty Earth Observatory, Columbia University*

Corresponding author: Maximilian Kotz, maxkotz@pik-potsdam.de

ABSTRACT: Projections of precipitation from global climate models are crucial for socioeconomic risk assessments under different emission scenarios, yet model discrepancies in the pattern and magnitude of future changes limit their application. Here, we show that using a pattern filtering technique can improve the accuracy with which the response of precipitation to anthropogenic forcing can be identified. Low-frequency component analysis is used to do so for four economically-relevant precipitation characteristics (mean intensity, wet day frequency, and extreme intensity and frequency) within individual CMIP-6 models. This approach improves agreement on the pattern of change by limiting the obscuring role of internal variability, but inherent model-biases remain considerable: 90% of models agree on the sign of change across 53, 36, 77, 66% of land area for each metric respectively. Despite these discrepancies in the sign of regional change, we find that differences in their average magnitude are well constrained by global surface warming (R^2 of 0.9, 0.89, 0.74, 0.77). Moreover, we show that these temperature-precipitation scaling relationships can be identified robustly within individual climate models from inter-temporal changes in the detected forced response (median R^2 of 0.83, 0.77, 0.82, 0.93). Inter-model spread in these relationships is considerable (coefficient of variation of 20-40%) and the differences between models often significant, thus diagnosing a source of the uncertainty in the magnitude of projected precipitation change. These results suggest that despite uncertainty in the spatial pattern, the magnitude of future precipitation changes is well constrained by temperature-scaling relationships both across and within climate models. These relations may offer a potential avenue to constrain the magnitude of future projections, as well as complementary information for impact assessments.

1. Introduction

The hydrological cycle is likely to play a key role in the socio-economic impacts of future climate change. Key determinants of social welfare, such as agricultural productivity (Liang et al. (2017)), flood damages (Davenport et al. (2021); Willner et al. (2018b)) and social stability (Hsiang et al. (2013); von Uexkull et al. (2016)) are closely linked to changes in precipitation. Moreover, recent work has delineated specific aspects of the distribution of precipitation which impact macroeconomic production, including annual totals, wet day frequency as well as the intensity and frequency of daily extremes (Damania et al. (2020); Holtermann (2020); Kotz et al. (2022)). Understanding how these characteristics of precipitation will change under anthropogenic influence is therefore crucial for informing risk assessments and climate policy. Climate models such as those in the Coupled Model Intercomparison Project (CMIP6; Eyring et al. (2016)) play a crucial role in this understanding, providing projections of precipitation under different levels of greenhouse forcing at the regional and temporal detail necessary for assessment of these impacts (Warszawski et al. (2014)). These projections can subsequently inform detailed assessments of the consequences of both mitigation (Lange et al. (2020); Thiery et al. (2021)) and adaptation (Willner et al. (2018a); Boulange et al. (2021)).

Despite recent progress, large uncertainties exist in projections of future precipitation change (Knutti and Sedláček (2013); Shepherd (2014)) which limit their utility in informing these impact assessments. From a global perspective, changes in average precipitation rates are constrained by the atmospheric energy budget to increase at a rate of 2-3%K^{-1} (Allen and Ingram (2002)). However, at the regional level the role of atmospheric circulation is important and complex, and changes in regional averages are less certain. Although particular components of circulation change, such as the weakening of the tropical Pacific circulation, are understood physically and have been detected clearly in models and historical observations (Held and Soden (2006); Vecchi and Soden (2007); Vecchi et al. (2006)), the resulting changes in precipitation can still be difficult to constrain because minor differences in the extent of shifting circulation can imply large differences in even the sign of regional precipitation change (Chadwick et al. (2016)). Consequently, dynamical changes from circulation remain a large source of the considerable uncertainty in projections of average regional precipitation (Chadwick et al. (2013); Ma and Xie (2013); Kent et al. (2015); Long et al. (2016); Shepherd (2014); Fereday et al. (2018)).

By contrast, changes in daily precipitation extremes are predominantly determined by thermodynamic effects relating atmospheric water vapour content to temperature (Allen and Ingram (2002); Fischer and Knutti (2016)). This thermodynamic contribution is simpler and hence more consistently projected across models (Pfahl et al. (2017)). Moreover, its dominance over circulation changes means that precipitation extremes have undergone a near-global increase which is well documented in historical observations (Min et al. (2011); Zhang et al. (2013); Fischer and Knutti (2016); Chen and Sun (2017); Kirchmeier-Young and Zhang (2020); Madakumbura et al. (2021)). Dynamical changes from atmospheric circulation cause only regional differences in the magnitude of these increases which constitute the majority of the projected uncertainty between models (Pfahl et al. (2017)).

To aid our understanding and application of precipitation projections, we here aim to explore their discrepancies in terms of both the spatial pattern and the magnitude of future regional changes. To maximise the applicability of our results for impact assessments, we focus on the changes over land of four key aspects of the distribution of precipitation from which impacts on economic production have been identified (Kotz et al. (2022)), namely: mean precipitation rates, wet day frequency and the intensity and frequency of daily extremes. We apply a pattern filtering technique (Wills et al. (2018, 2020)) to separate the forced response to anthropogenic influence from internal variability separately within each member of a multi-model CMIP-6 ensemble. This approach accounts for spatio-temporal correlations while detecting the forced response, aiming to limit the obscuring role of internal variability and hence improve our assessment of inter-model discrepancies. This is of particular importance given the relatively strong internal variability present in precipitation characteristics (Deser et al. (2014)).

Our approach improves agreement between models on the spatial pattern of the forced response, but inherent model discrepancies remain considerable, in particular for mean precipitation and wet day frequency. However, we find that the magnitudes of regional change are very well constrained by the extent of global mean temperature (GMT) change. Interestingly, these relationships are improved when the absolute value of regional precipitation change is assessed, considerably so for mean precipitation and wet day frequency. This suggests that although models may disagree on the sign of regional change, particularly for precipitation characteristics which are dominated by uncertain circulation changes, the magnitude of such change is well constrained by the underlying

thermodynamic forcing of the climate system i.e. GMT changes. We further demonstrate that these temperature-precipitation scaling relations are robustly identifiable within individual climate models from inter-temporal changes in the detected forced response. The rates at which precipitation changes scale with GMT show considerable and significant differences between models, thus diagnosing a source of the uncertainty in the magnitude of projected precipitation change, and offering a potential avenue to constrain them.

2. Data and Methods

a. CMIP6 data

We use daily surface precipitation rates and daily 2-m temperature from 21 climate models participating in CMIP6. We choose models which provide output under both the historical (1850-2014) and the future (2015-2100) greenhouse forcing scenarios specified by SSP126 and SSP585. A full list of models is displayed in Figs. A1-4.

b. Precipitation indices

Our assessment of precipitation change focuses on a number of key characteristics of the distribution of daily precipitation which have been demonstrated to have significant impacts on macroeconomic production (Kotz et al. (2022)). Therefore, the following four annual precipitation indices are calculated from daily precipitation rates on the native grids of each CMIP6 model over land: the annual mean precipitation rate (calculated over all days),

$$Pm_{x,y} = \frac{1}{N_y} \sum_{d=1}^{N_y} P_{x,d} \tag{1}$$

the annual frequency of wet days (defined using a 1mm threshold),

$$Pwd_{x,y} = \sum_{d=1}^{N_y} H(P_{x,d} > 1mm) \tag{2}$$

the annual daily maximum as a measure of the intensity of daily extremes,

$$PX1_{x,y} = \max(P_{x,d} : x = 1, ...N_y) \tag{3}$$

and the annual number of days exceeding the 99^{th} percentile of the historical distribution, $99p$, (historical percentiles calculated over all days from 1850-1950) as a measure of the frequency of daily extremes,

$$P > 99p_{x,y} = \sum_{d=1}^{N_y} H(P_{x,d} > 99p) \tag{4}$$

where N_y is the number of days in a given year and H is the Heaviside step function, and x and d respectively denote grid-cell and day. These annual measures are estimated on the native CMIP grids, before being linearly interpolated to a common 1-by-1 degree grid for further analysis.

c. Separating the forced response from internal variability: low-frequency component analysis

Identifying the forced response of the climate system to anthropogenic influence is complicated by natural internal variability (Deser et al. (2012)), particularly on the multi-decadal time-scales over which averages are often used to characterise a forced response (Masson-Delmotte et al. (2021)). One approach to overcome this issue is to use large ensembles of a single climate model in which internal variability can be characterised and removed by initialising ensemble members from different initial conditions (Kay et al. (2015)). However, to consider the full range of structural differences between models which can bias the forced response, a variety of climate models must be assessed. We do so using the multi-model ensemble CMIP6, and instead apply a pattern filtering technique to individual ensemble members to separate the forced response from internal variability. Low-frequency component analysis (LFCA) takes advantage of the different time-scales of the respective processes to identify the forced response from a single realisation with accuracy comparable to ensembles with up to 20 realisations (Wills et al. (2020)). We use LFCA over other methods, such as signal-to-noise maximising pattern-filtering, because of its superior performance in detecting the forced response from a single realisation (Wills et al. (2020)).

Here we provide a conceptual summary of LFCA and of its application to identifying the climatic response to anthropogenic forcing, please see Wills et al. (2018) for a more detailed introduction to and description of the method. LFCA is a form of linear-discriminant analysis which identifies independent modes which can account for the greatest ratio of low-frequency to total variance. Given the longer time-scales over which changes due to greenhouse forcing evolve in comparison

to those due to internal variability, this form of variance maximisation can accurately separate the two (Wills et al. (2018, 2020); Kotz et al. (2021)).

Linear recombinations of the leading empirical-orthogonal-functions, (EOFs) are found which maximise this variance ratio. We retain a sufficient number of EOFs to account for a minimum of 70% of the original spatio-temporal variance, and define low-frequency variance as that resulting from applying a 20-year low-pass Butterworth filter with reflecting boundary conditions to grid-cell level departures from linear trends. We use a lower cut-off frequency than Wills et al. (2018, 2020), due to the lower signal-to-noise ratio of the climate change signal in precipitation than temperature (Deser et al. (2014)), but recover consistent results under alternative filtering specifications. The resulting linear recombinations are independent, and ordered in terms of increasing frequency. They constitute both a "low-frequency component" (LFC) and "low-frequency pattern" (LFP); the LFC is a time-series which describes the temporal evolution of the specific spatial pattern encompassed by the LFP. Given the longer time-scales over which anthropogenic forcing evolves compared to internal variability, we interpret the lowest-frequency component as the response to anthropogenic forcing, following Wills et al. (2020) and Kotz et al. (2021).

We apply LFCA to the four precipitation indices (over land areas) and to annual mean temperature (over the globe) from 1950-2100 under the anthropogenic forcing of the historical period and both the SSP126 and SSP585 future scenarios, having first linearly interpolated each index to a common 1-by-1 degree grid. The forced change between two given time periods (usually between two decades) is then calculated as the product of the lowest-frequency LFP and the difference between temporal (usually decadal) averages of the corresponding LFC.

In a number of cases, we also estimate the forced changes in each precipitation metric using temporal averages of the data prior to any detection with LFCA. In these cases we either use 10 (Fig. 2 and B6-B9) or 30 year periods (Fig. 2) to estimate the change.

d. Scaling between the magnitude of precipitation changes and temperature change

To estimate the average magnitude of regional precipitation change, continental, area-weighted averages of the absolute regional change are calculated from the forced patterns of precipitation change identified with LFCA. For the extreme metrics, the regional changes are assessed in terms of percentage change from the historical (1850-1950) baseline in order to make comparison to

the theoretical expectations of the Clausius-Clapeyron relation. These land-area averaged absolute precipitation changes are then compared to estimates of the change in global mean temperature, calculated from the global-area average change in 2-m surface temperature estimated from the lowest-frequency component identified comparably with LFCA. In Fig. 4, changes in precipitation and temperature between 1950-1960 and 2090-2100 are compared between models. In Fig. 5 changes between pairs of non-overlapping decades separated by 25-years within each individual model are used.

Linear scaling rates are estimated with a least-squares linear regression for mean precipitation and the number of wet days. Due to the theoretical expectations of the Clausius-Clapeyron relation for the extreme metrics, in these cases an exponential scaling is estimated by transforming the percentage precipitation changes, $\frac{\delta P}{P}$, into a logarithmic form, $log(\frac{\delta P}{P} + 1)$. Methodological uncertainty in the estimates of these scaling rates is obtained via a bootstrapping approach. In Fig. 4, the selection of climate models is re-sampled 1000 times with replacement, whereas in Fig. 5 the different time periods are re-sampled equivalently. As such, these estimates reflect the methodological uncertainty arising from the available variety of climate models (in Fig. 4) and the variety of forcing occurring over the different periods of the available scenarios (in Fig. 5). When estimating the significance of differences between model scaling rates, we estimate a distribution of differences between model scaling rates from the 1000 re-sampled estimates, and assess whether the 95% confidence intervals of this distribution of differences encase zero.

3. Results

a. Detection of the precipitation response to anthropogenic-forcing in individual climate models

We identify the response of mean daily precipitation, wet day frequency and the intensity and frequency of daily extremes to anthropogenic forcing (historical and SSP585) within individual CMIP6 climate models using LFCA. Fig. 1 shows results for a selection of five models (see Figs. A1-4 and A5-8 for results from all members of the ensemble under SSP585 and SSP126 forcing respectively). For each precipitation index and for each model, the lowest-frequency component (LFC-1) exhibits a near-monotonic trend which closely follows the increasing concentrations of greenhouse gases in the historical and SSP585 scenario. However, both the intensity and spatial pattern of the detected end-of-century forced change (1950-60 to 2090-2100) show clearer

differences between models. Maps of the forced-change are displayed separately for each model to present the heterogeneity of modelling bias (see Figs. A1-4 for results from all models).

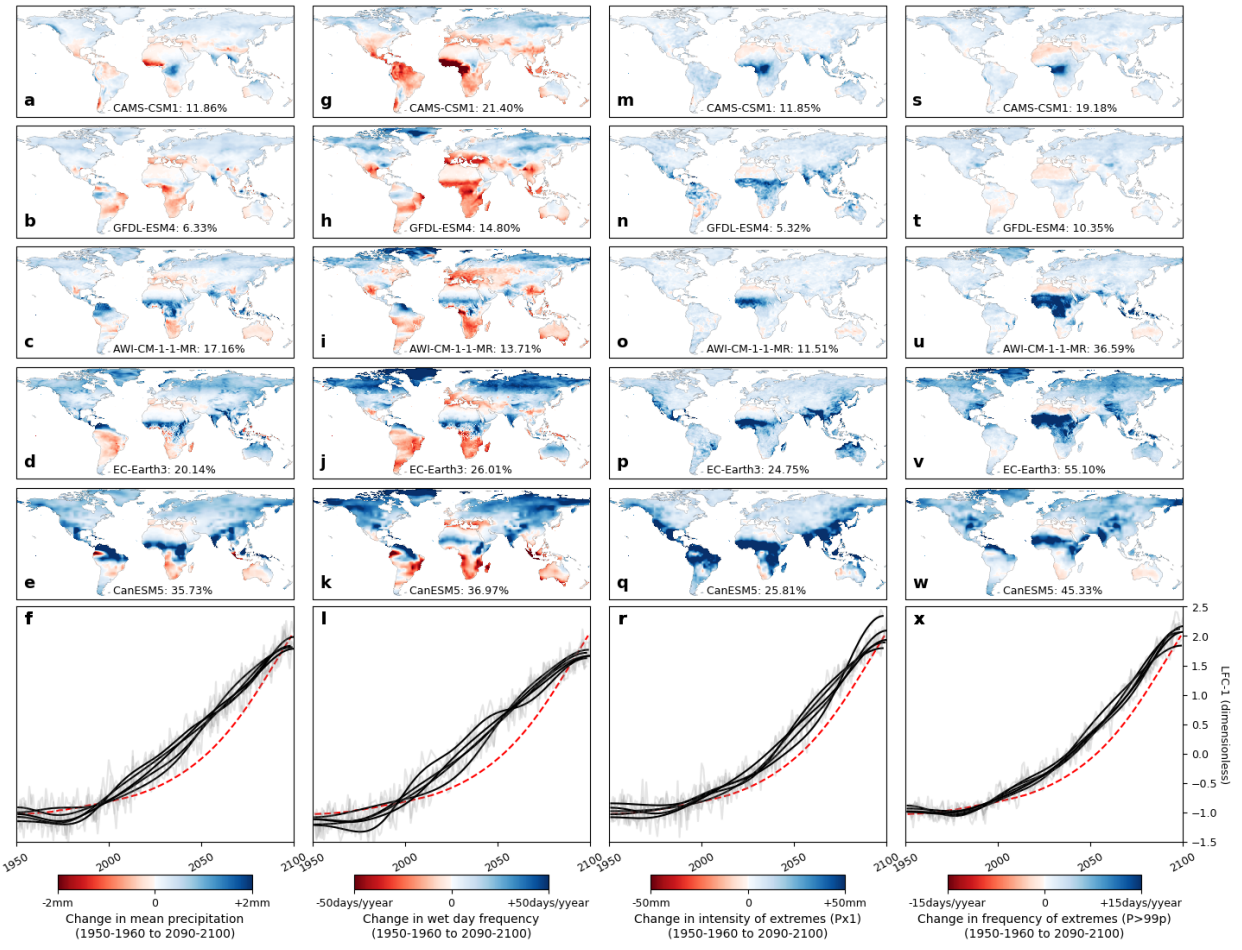

FIG. 1. The forced response of four precipitation characteristics to historical (1950-2014) and future (SSP585, 2015-2100) anthropogenic forcing, detected in individual CMIP6 climate models with low-frequency component analysis. (a-e) The spatial pattern of the forced change in mean precipitation from 1950-60 to 2090-2100 (the product of the lowest-frequency pattern with the difference between decadal averages of its corresponding component) for a selection of models (see Fig. S1 for all 21 members of the CMIP-6 ensemble). (f) The temporal evolution of the lowest-frequency components (LFC-1) of mean precipitation change are shown in grey with a 20-year Butterworth filtered time-series in black. Time series for each model are overlain due to their similarity. The concentration of greenhouse gases in the historical and SSP585 are rescaled and shown in red for comparison. Corresponding results for changes in wet day frequency (g-l), the intensity of daily extremes (m-r) and the frequency of daily extremes (s-x) are shown alongside. Models are ordered top to bottom in terms of their respective GMT change. The model name is indicated in the bottom of each panel, along with the percentage of total spatio-temporal variance accounted for by LFC-1.

b. The spatial patterns of forced change - intermodel uncertainty

We explore the extent of these biases in the modelled response of precipitation to anthropogenic forcing in Fig. 2, which shows the fraction of land area on which at least a certain proportion of models agree on the sign of forced change. Agreement is larger for the extreme metrics than for mean precipitation and the frequency of wet days, consistent with our expectations given the large contribution of uncertainty in the circulation response to discrepancies in changes in mean conditions (Shepherd (2014); Chadwick et al. (2016)). Agreement is also larger in the detected response to SSP585 forcing compared to SSP126, reflecting the fact that the stronger greenhouse forcing in the former generates a larger signal-to-noise ratio (i.e. the magnitude of the forced precipitation response compared to that of natural internal variability) which aids the detection of the forced response.

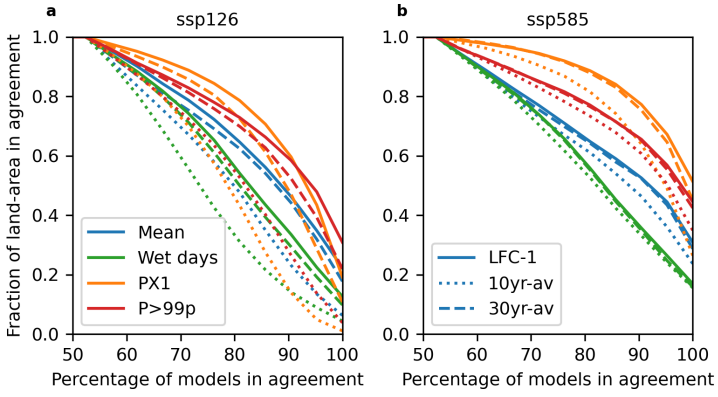

FIG. 2. The extent of inter-model agreement in the spatial pattern of forced precipitation change. The land area on which at least a certain percentage of models agree on the sign of forced change is shown for mean precipitation, the frequency of wet days, and the intensity (PX1) and frequency of daily extremes (P>99p). Results are shown having detected the forced response separately using low-frequency component analysis (LFC-1), and multi-decadal averages (10yr-av, 30yr-av).

Comparing the extent of agreement between detection methods, we find that using LFCA reduces inter-model discrepancies compared to taking decadal averages. These improvements are most considerable under the SSP126 forcing scenario, in which notable improvements are made even on a 30-year average. Assuming that inter-model agreement constitutes a benchmark of accuracy, this suggests that accounting for spatio-temporal correlations during detection via LFCA can improve

the accuracy with which a forced response is detected, and that these improvements are most considerable in contexts where the signal-to-noise ratio is low.

Despite these improvements, discrepancies between models in the sign of forced change persist. This is particularly so for changes in mean conditions, where high agreement (90% of models) is found on only 53 and 36% of land area for mean precipitation and wet day frequency under SSP585. By contrast high agreement is found on 77 and 65% of land area for the intensity and frequency of daily extremes under SSP585. The spatial distribution of these discrepancies is shown in Fig. 3 overlain on maps of the ensemble mean forced response.

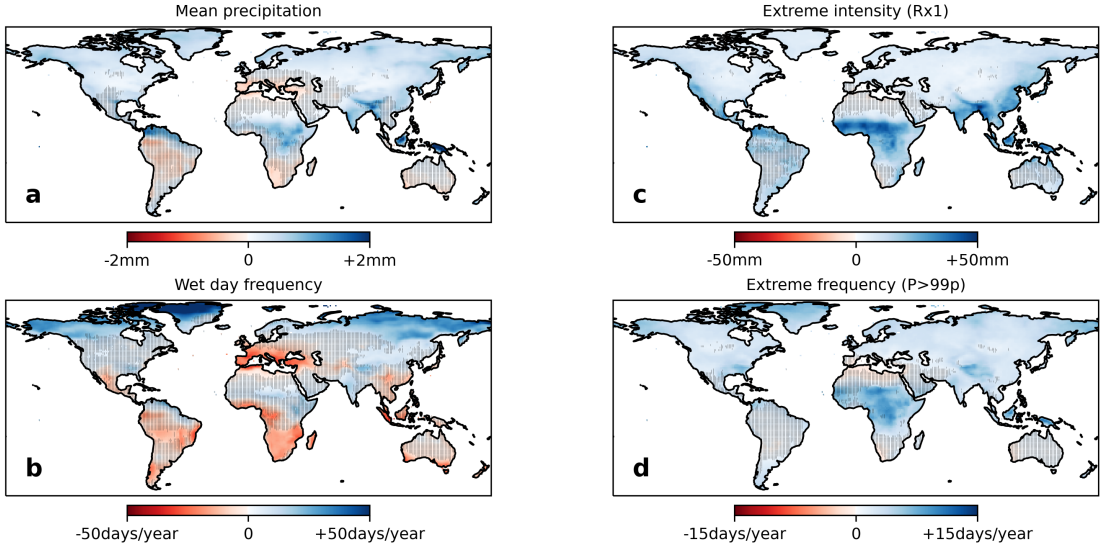

FIG. 3. The ensemble-mean forced response of mean daily precipitation (a), wet day frequency (b), and the intensity (c) and frequency (d) of daily extremes to SSP585 forcing. Forced changes are calculated with LFCA as described in the caption to Figure 1. Hatching indicates grid-cells in which less than 90% (19/21) of the ensemble agree on the sign of change.

The ensemble-mean forced response of precipitation (Fig. 1) resembles that identified by the IPCC (Masson-Delmotte et al. (2021)). Increases in mean precipitation across most of the global land mass contrast decreases across the Mediterranean basin, Central South America, and the southern tips of Africa and Australia. These changes reflect both a zonal intensification of the hydrological cycle (wet-get-wetter) (Marvel and Bonfils (2013)) and regional circulation changes (Chadwick et al. (2013)). The response of the number of wet days follows this pattern, but with

considerably more wide-spread regional reductions. This difference likely reflects the expected shift of the distribution of precipitation from relatively lighter to heavier events under global warming (Allen and Ingram (2002); Fischer and Knutti (2016)). The extreme indices demonstrate a response with more homogeneous increases, although some reductions are found. Reductions generally occur in regions of large mean precipitation decrease and large uncertainty, matching those identified by Pfahl et al. (2017) as having large dynamical contributions from circulation change which oppose the general thermodynamic increase in extreme precipitation.

c. The magnitude of forced change - temperature-precipitation scaling across models

Despite persistent uncertainty in the projected sign of regional precipitation change, we find that the average magnitude of such change scales strongly with GMT across all metrics (Fig. 4). To demonstrate this, we assess the land-area averaged (excluding Antarctica) absolute change in each precipitation metric from the forced response which we detect in each model, as well as the global-area averaged temperature change in each model estimated comparably using LFCA. Taking absolute values improves the correlations between precipitation and GMT change (compare Fig. 4 to Fig. B1), considerably so for mean precipitation and the frequency of wet days. This suggests that when shifting atmospheric currents contribute large uncertainty to the sign of regional precipitation change, the intensity of these changes can still be closely related to the underlying thermodynamic driver. We note that taking absolute values is a similar approach to that used by Chadwick et al. (2016), who assess the percentage of tropical land area projected to experience considerable precipitation (>20%) of either positive or negative sign. Our method offers a complementary perspective by assessing the average magnitude of change across all land-areas in multiple metrics.

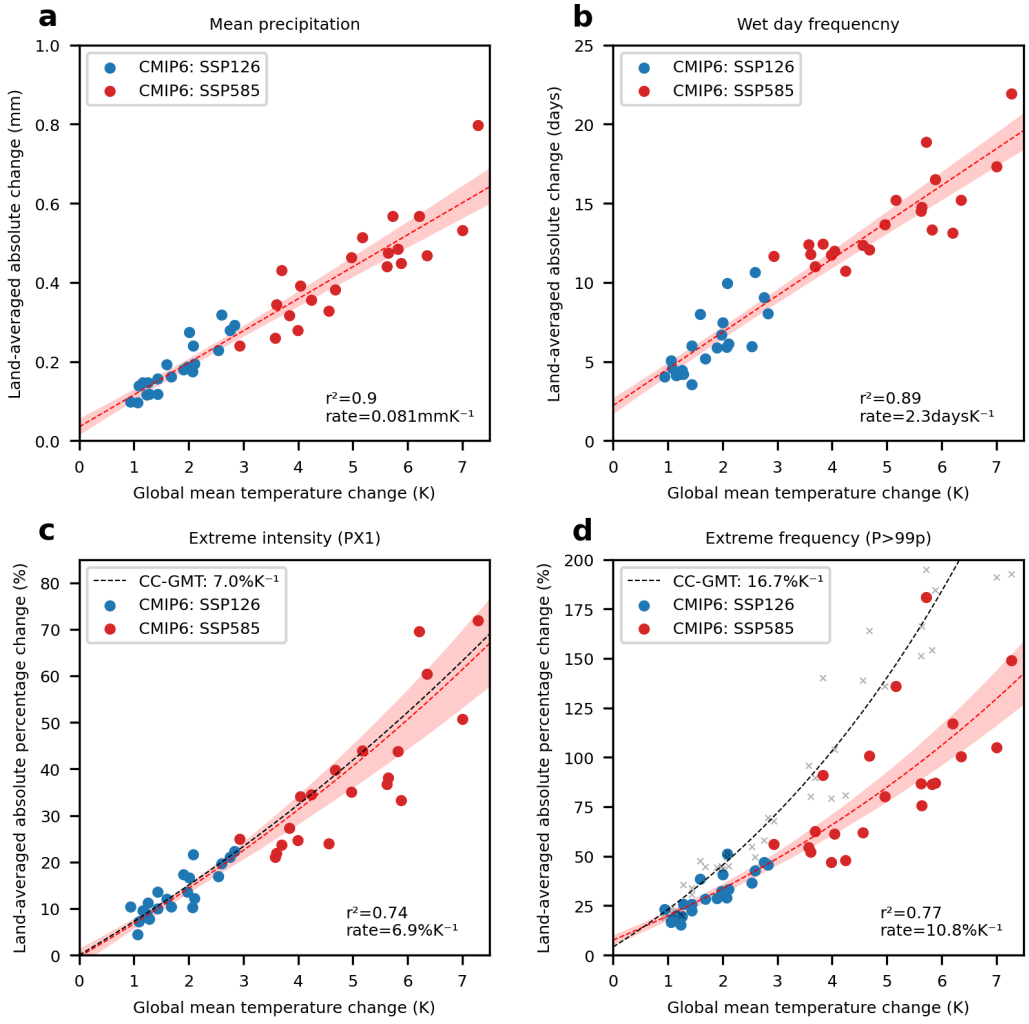

FIG. 4. The scaling of land area-averaged absolute precipitation change with global mean temperature (GMT) across CMIP6 models and scenarios. Forced changes between 1950-1960 and 2090-2100 are calculated from the lowest-frequency component of each precipitation index (as in Fig. 1) and of annual mean temperature. Red and blue colors denote the SSP585 and SSP126 scenarios of future greenhouse forcing. The results of least-squares linear regressions are shown in dashed red with the 5^{th} and 95^{th} confidence intervals shaded based on bootstrapped estimates of the regression (1000 climate model resamples with replacement). Changes in extreme metrics are calculated as a percentage of the historical baseline (1850-1950) for comparison to the theoretical expectations of the Clausius-Clapeyron relation, shown in dashed black lines. For the frequency of daily extremes (P>99p), the CC relation is estimated by scaling up each day of the historical precipitation distribution (1850-1950) by the given level of GMT change, and re-calculating each index, following Fischer and Knutti (2016). Individual estimates from this method are shown in grey, the black dashed-line showing the result of an exponential regression to these estimates. The resulting theoretical scaling rate of this regression is displayed in the figure legend.

We express changes in the extreme metrics in terms of percentages from the historical baseline (1850-1950, percentages calculated at the grid-cell before spatial aggregation) in order to compare them to the theoretical expectations of the Clausius-Clapeyron (CC) relation. We find that the intensity of extremes follow this behaviour closely, increasing at a rate of $6.9\%K^{-1}$. For the frequency of daily extremes, we follow Fischer and Knutti (2016) to estimate a theoretical thermodynamic scaling. We apply the CC relation for a given GMT change to each day of the historical precipitation distribution (1850-1950) and then re-calculate the indices on the re-scaled distribution. This predicts a considerably higher scaling of $16.7\%\mathrm{K}^{-1}$. Although, we observe a larger scaling for the frequency rather than the intensity of extremes, it falls short of this expected scaling at $10.8\%\mathrm{K}^{-1}$.

d. Temperature-precipitation scaling within models

Furthermore, we exploit the detection of a forced precipitation response within each individual CMIP-6 model to assess the scaling of precipitation and GMT change within individual models. To do so, we use changes in the time-varying forced response of precipitation and temperature occurring over pairs of non-overlapping decades separated by 25 year periods within each climate model. This approach reveals robust temperature-precipitation scaling relationships which are clearly identifiable within each climate model, and which can explain a large proportion of the inter-temporal changes in precipitation (Fig. 5). Considerable improvements in the robustness of these estimates are made when first filtering with LFCA compared to using the raw CMIP data, in particular for mean precipitation and the number of wet days. Using LFCA, the R^2 of the identified relations increase from median values of 64, 4, 77 and 82% to 84, 76, 84 and 93% for mean precipitation, wet day frequency and the intensity and frequency of daily extremes respectively (see Figs. B6-B9 for the scalings identified without LFCA).

On average, the rates at which precipitation changes scale with GMT within individual models is consistent with that identified between models (Fig. 6), other than for the frequency of extremes for which a considerably larger scaling is observed on average within models (15.21%) which has closer consistency to the expected CC-scaling . However, there is considerable inter-model heterogeneity in these rates, the distribution of which is shown in Fig. 6. We estimate coefficients of variation of 21, 19, 39 and 28% for the distributions for mean precipitation, wet day frequency and the intensity and frequency of daily extremes. This demonstrates that large inter-model uncertainty exists in the modelled rate at which precipitation changes scale with temperature. Moreover, the inter-model differences in intra-model scaling rates are significantly different from zero at the 5% level given our methodological uncertainty (estimated using 1000 bootstrapped replacements of the inter-temporal changes in the regressions estimated in Fig. 5) for 37, 29, 56 and 61% of unique model pairs for mean precipitation, the number of wet days and the intensity and frequency of extremes respectively. As such we can conclude that there are significant inter-model differences in the rates at which precipitation scales with GMT, particularly for the scaling of extremes. These differences contribute to uncertainty in the projections of future precipitation change, and their identification therefore offers the opportunity to constrain such uncertainties. One potential avenue to do so could be the use of observational estimates of the rate of these scalings to constrain multi-model ensemble projections.

Exploring the source of these diverging precipitation scaling rates is beyond the scope of this analysis, but we note that there is clear co-variation between the GMT-scaling rates of mean precipitation and both of the extreme metrics across models (Fig. B10). This suggests that common physical mechanisms may underlie the model biases in the rates at which these precipitation characteristics scale with GMT.

4. Discussion and concluding remarks

Our work sheds light on a number of challenges relating to the uncertainty of future precipitation projections. First, we demonstrate that the use of a pattern-filtering technique, LFCA, can improve the accuracy with which the spatial patterns of anthropogenically-forced precipitation change are projected by limiting the obscuring role of internal variability, in particular in the context of low signal-to-noise ratios. However, considerable uncertainties persist, reflecting the discrepancies

inherent in the modelling of physical processes within different climate models. Previous work suggests that the dynamical contribution from atmospheric circulation change is the major source of these uncertainties (Shepherd (2014); Kent et al. (2015); Pfahl et al. (2017)), and continued work to understand and reduce them is crucial.

Despite these uncertainties, our analysis demonstrates that the magnitudes of precipitation change are closely constrained by changes in GMT. While the scaling of precipitation extremes with GMT across climate models has already been studied, such robust scaling of changes in mean conditions have not previously been identified. Our approach taking absolute values of regional change contributes considerably to revealing these relations. This approach relates closely to that of Chadwick et al. (2016), but demonstrates precipitation-GMT scaling for the magnitude rather than extent of change, and considers multiple metrics across the global land area rather than averages across the tropics. The fact that these relations are improved when taking absolute values, and most considerably so for the metrics in which dynamical changes from atmospheric circulation contribute large uncertainty to the sign of regional change, suggests that the intensity of such dynamical changes may also be well constrained by the underlying thermodynamic driver of climatic change i.e. GMT. The observed dependence of shifting atmospheric circulation on changes to sea surface temperature and land-sea temperature-gradients (Deser and Phillips (2009); Chadwick et al. (2013, 2014); Ma and Xie (2013)) may support such an interpretation, but further analysis in this regard is beyond the scope of the present work. Regardless, these relations suggest that uncertainty in the magnitude of regional precipitation change is closely tied to uncertainty in the equilibrium climate sensitivity and GMT change.

Furthermore, by identifying these scaling relations clearly within individual climate models, we are able to diagnose a source of the uncertainty in the magnitude of projected precipitation change, in addition to that arising from uncertainty in GMT. The rates at which precipitation scales with GMT differ considerably and significantly between models, and this could present opportunities to constrain the magnitude of future projections by their comparison to estimates of such scalings from observations. Accurate observational estimates may be challenging to obtain given a relatively short historical record during which different components of anthropogenic forcing (aerosol, greenhouse) may confound one another, amongst other challenges (Williamson et al. (2021)). Nevertheless, observational constraints on precipitation have shown some success

(O'Gorman (2012); Shiogama et al. (2022); Schewe and Levermann (2022)), and the clear signal of intensification of precipitation extremes in the historical record may suggest that such scalings are indeed accurately identifiable (Min et al. (2011); Zhang et al. (2013); Fischer and Knutti (2016); Chen and Sun (2017); Kirchmeier-Young and Zhang (2020); Madakumbura et al. (2021)). Analyses of precipitation extremes in Europe suggest that CMIP models may strongly under-estimate the observed change for a given level of warming (Fischer and Knutti (2016); Myhre et al. (2019)), emphasising that constraining such projections in this way may be critical.

Finally, the demonstrated constraints on the magnitude of future precipitation change may be useful for global risk and impact assessments. Accurate information on the sign and magnitude of regional changes is undoubtedly of the greatest value, but in the absence of the former a constraint on the latter may provide some complementary information. For example, global risk assessments may find utility in constraints on the global average magnitude of expected impacts from precipitation changes e.g. in terms of how they compare to impacts from other aspects of climate change (such as from temperature) or to other socio-economic events such as pandemics, wars or financial crises. Moreover, the demonstration of such robust scalings may support the use of pattern scaling techniques (Herger et al. (2015)) in the projection of precipitation impacts. This would constitute a key step within the complex chain linking emissions, to GMT change, to the impacts arising from regional precipitation change (Kotz et al. (2022)).

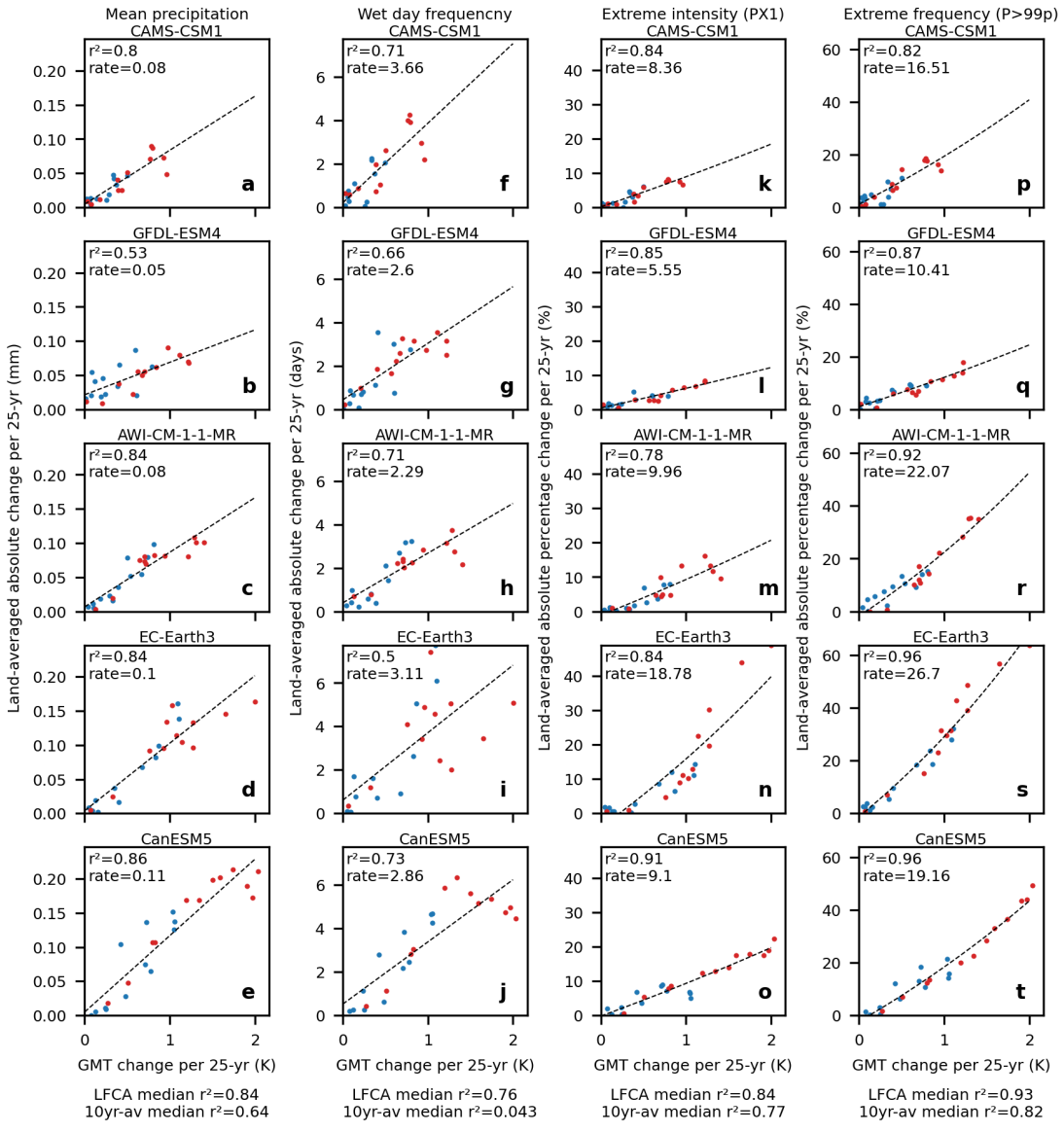

FIG. 5. The scaling of the land-area averaged absolute change of precipitation characteristics with global mean temperature (GMT) change within individual CMIP6 climate models. A selection of models are shown for simplicity, but results for the full ensemble can be seen in Figs. B2-5. Forced changes are calculated from the lowest-frequency component detected with low-frequency component analysis, and the scalings identified from changes between pairs of non-overlapping decades separated by 25 years. Red and blue colors denote the SSP585 and SSP126 scenarios of future greenhouse forcing and in black the results of a least-squares regression are shown. Models are ordered (a-u, top-left to bottom-right) from lowest to highest GMT change as in Fig. 1. The median R^2 obtained across climate models is indicated at the bottom of each column, having detected the forced changes using either LFCA or decadal averages. See Figs. B6-9 for the results without having first applied LFCA.

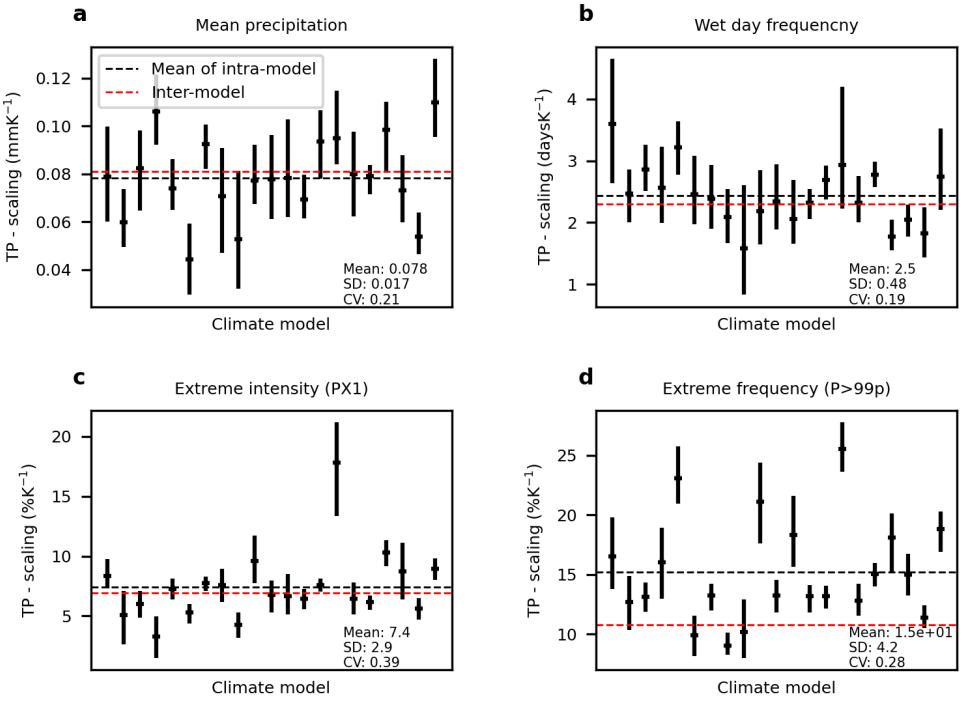

FIG. 6. Inter-model spread in the temperature-precipitation scaling relationships identified from the forced changes detected within individual CMIP6 models, for (a) mean precipitation, (b) wet day frequency and (c) the intensity (Px1) and (d) frequency (P>99p) of daily extremes. 10% confidence intervals of the scaling within each model are obtained by boot-strapping the regressions shown in Fig. 5, and displayed as vertical bars. The mean of the within-model scalings (as identified in Fig. 5) and the between-model scalings (as identified in Fig. 4) are displayed by the horizontal dashed lines in black and red respectively. The mean, standard deviation, and coefficient of variation of the intra-model scalings across models are also displayed numerically.

Acknowledgments. MK and LW received funding from the Volkswagen foundation. SL received funding from the German Research Foundation (DFG, project number 427397136) and from the German Federal Ministry of Education and Research (BMBF, project number 01LP1907A). AL received funding from the Horizon 2020 Framework Programme of the European Union (grant agreement number 820712).

Data availability statement. Raw CMIP6 data is available from https://esgf-node.llnl.gov/projects/cmip6/. Code for low-frequency component analysis is available from https://github.com/rcjwills/lfca. All other data and code is available form the authors upon request.

APPENDIX A

Forced response detected with LFCA

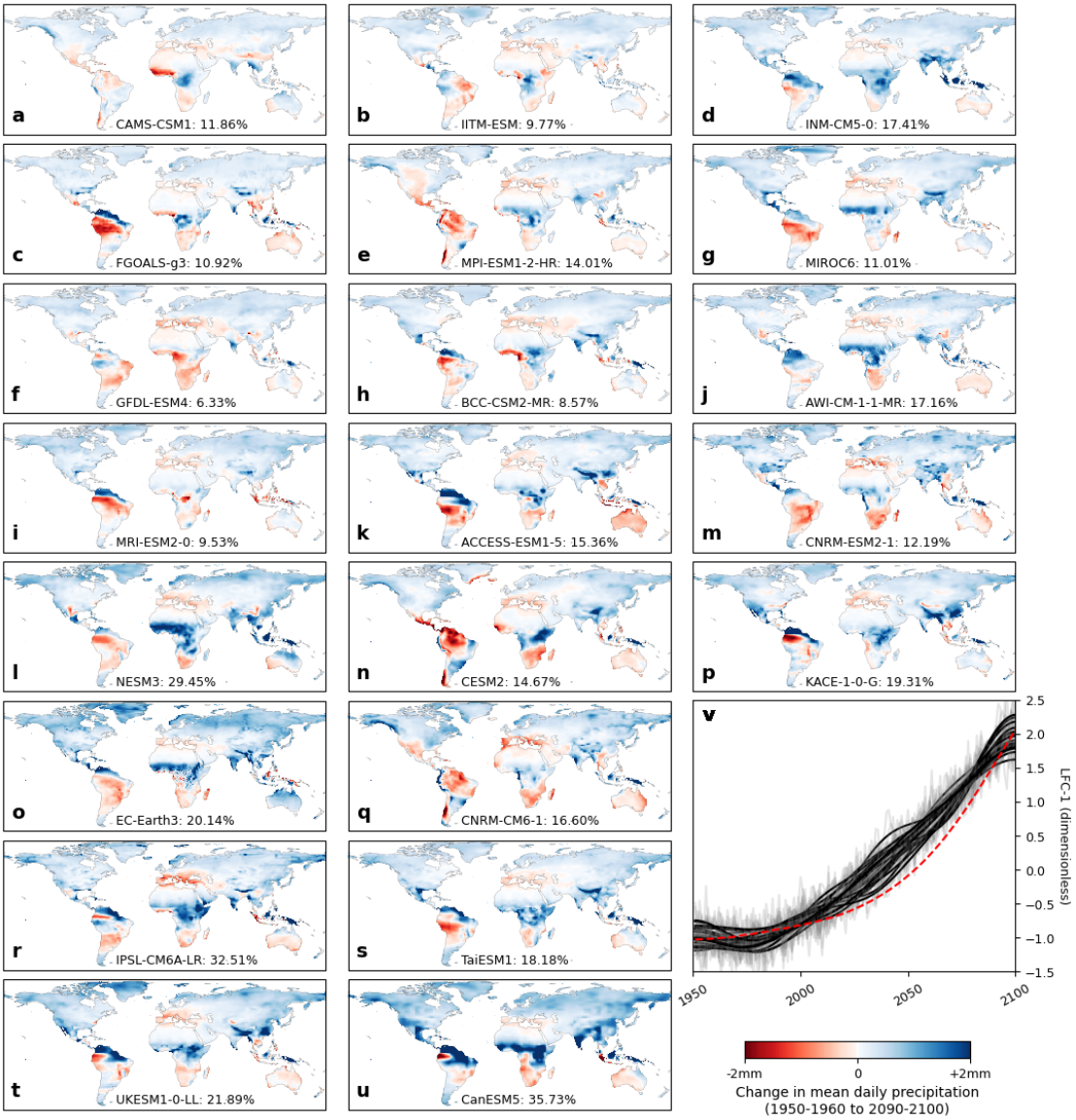

FIG. A1. The detected forced response of mean precipitation under historical and SSP585 scenario greenhouse forcing. As Fig. 1 but for all models in the CMIP6 ensemble. Models are ordered a-u in order of increasing GMT change.

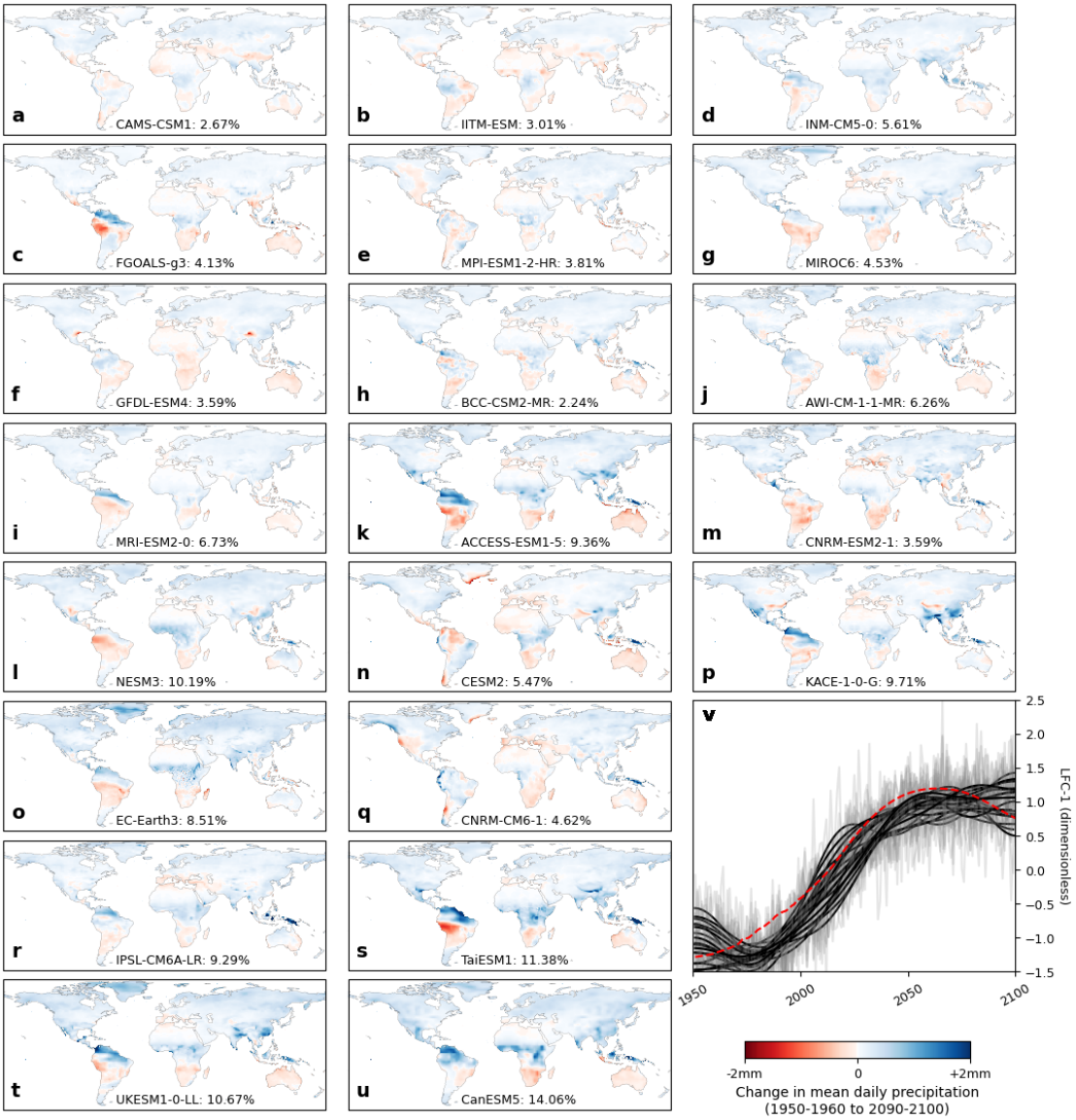

FIG. A2. As Fig. A1 but under the historical and SSP126 scenario greenhouse forcing.

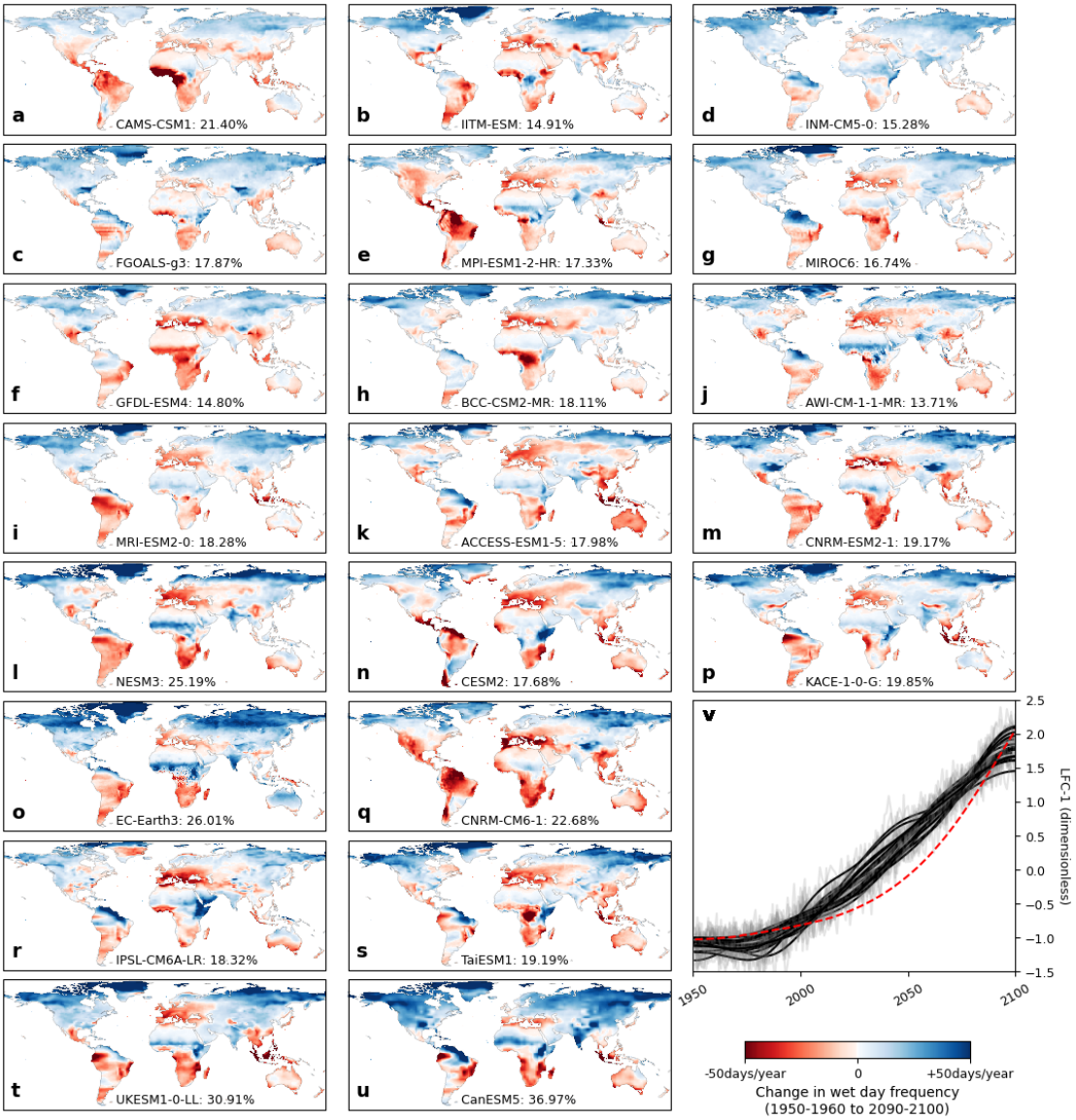

FIG. A3. The detected forced response of the wet day frequency under historical and SSP585 scenario greenhouse forcing. As Fig. 1 but for all models in the CMIP6 ensemble. Models are ordered a-u in order of increasing GMT change.

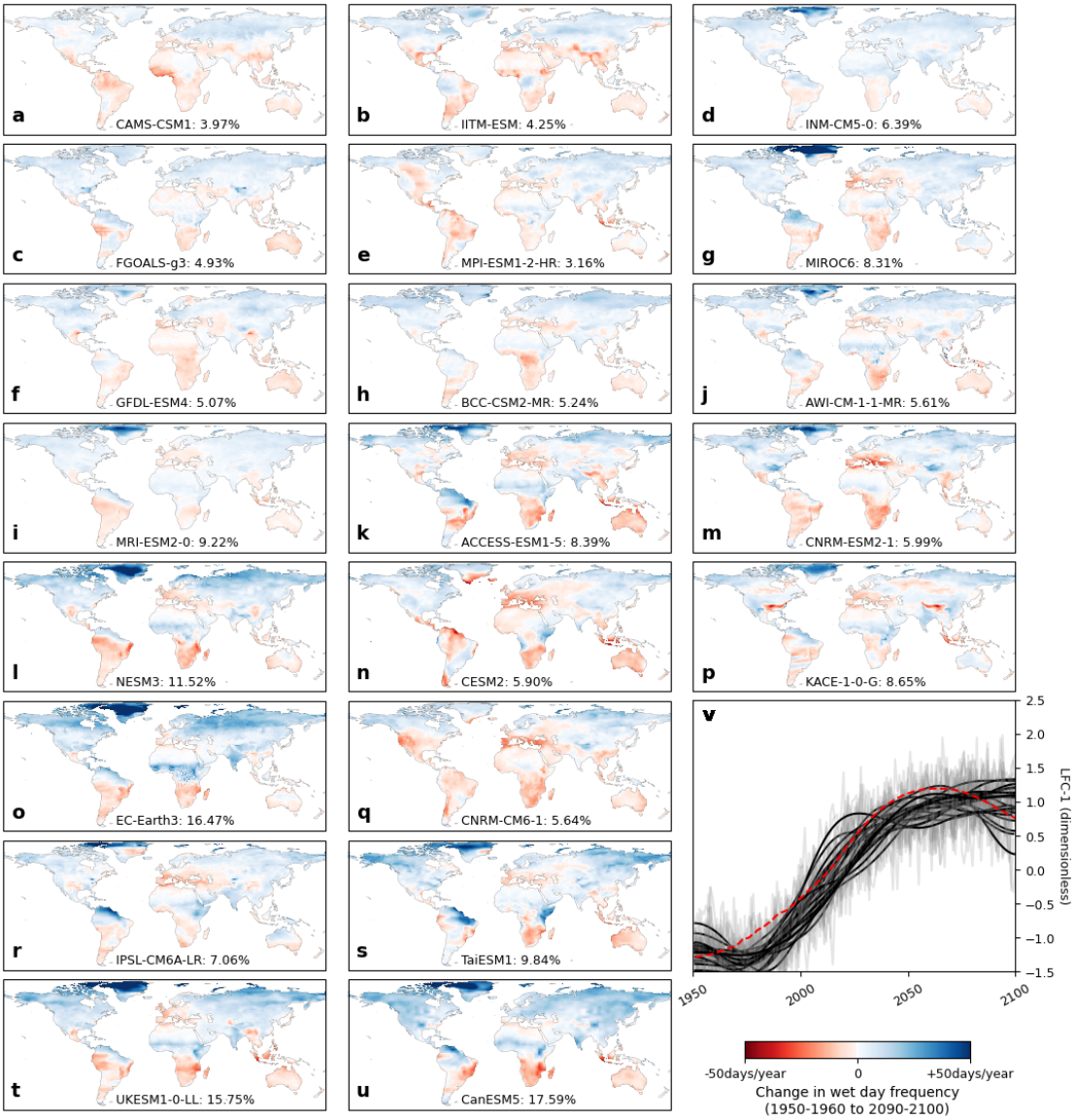

FIG. A4. As Fig. A3 but under the historical and SSP126 scenario greenhouse forcing.

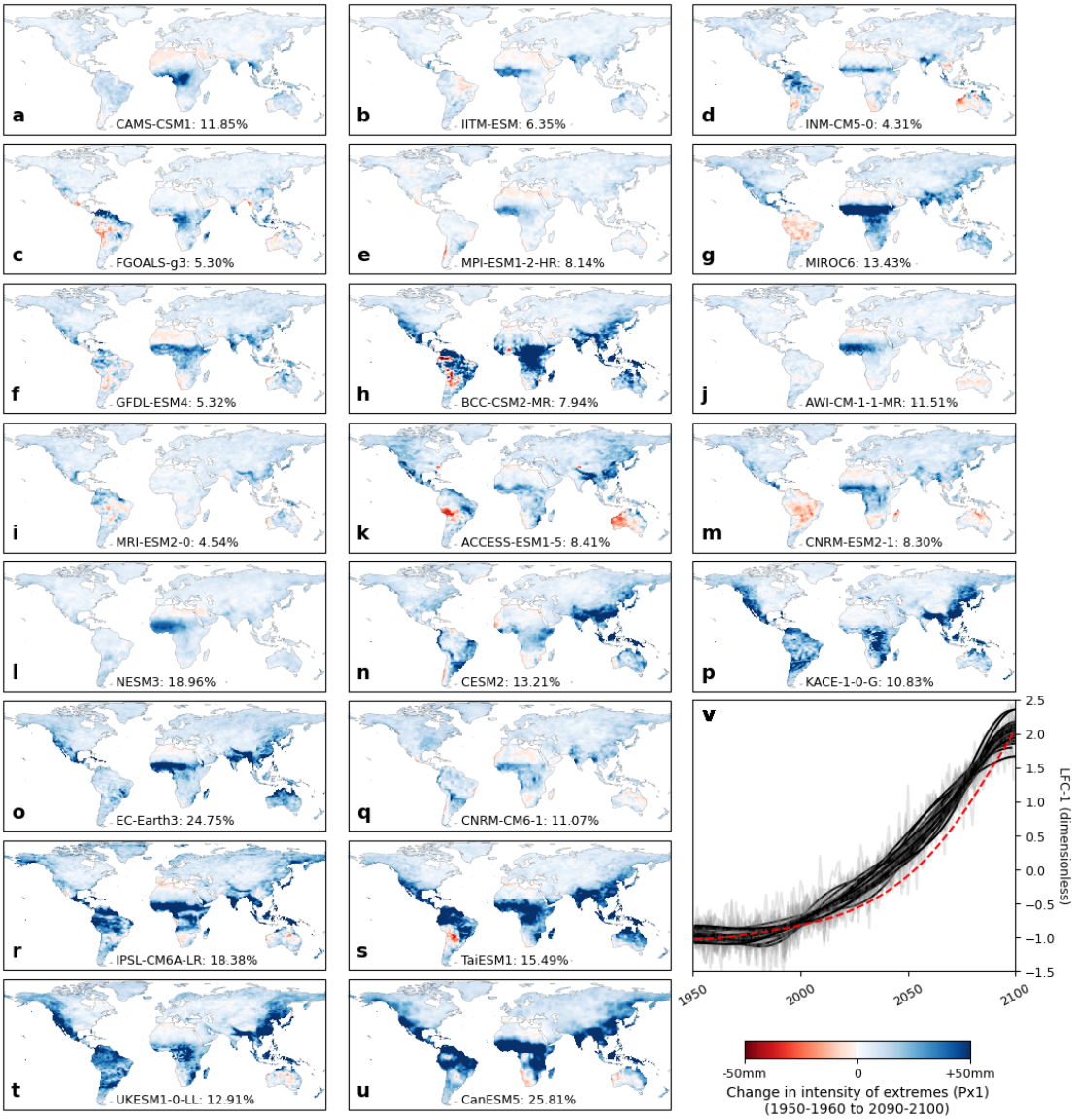

FIG. A5. The detected forced response of the intensity of daily extremes under historical and SSP585 scenario greenhouse forcing. As Fig. 1 but for all models in the CMIP6 ensemble. Models are ordered a-u in order of increasing GMT change.

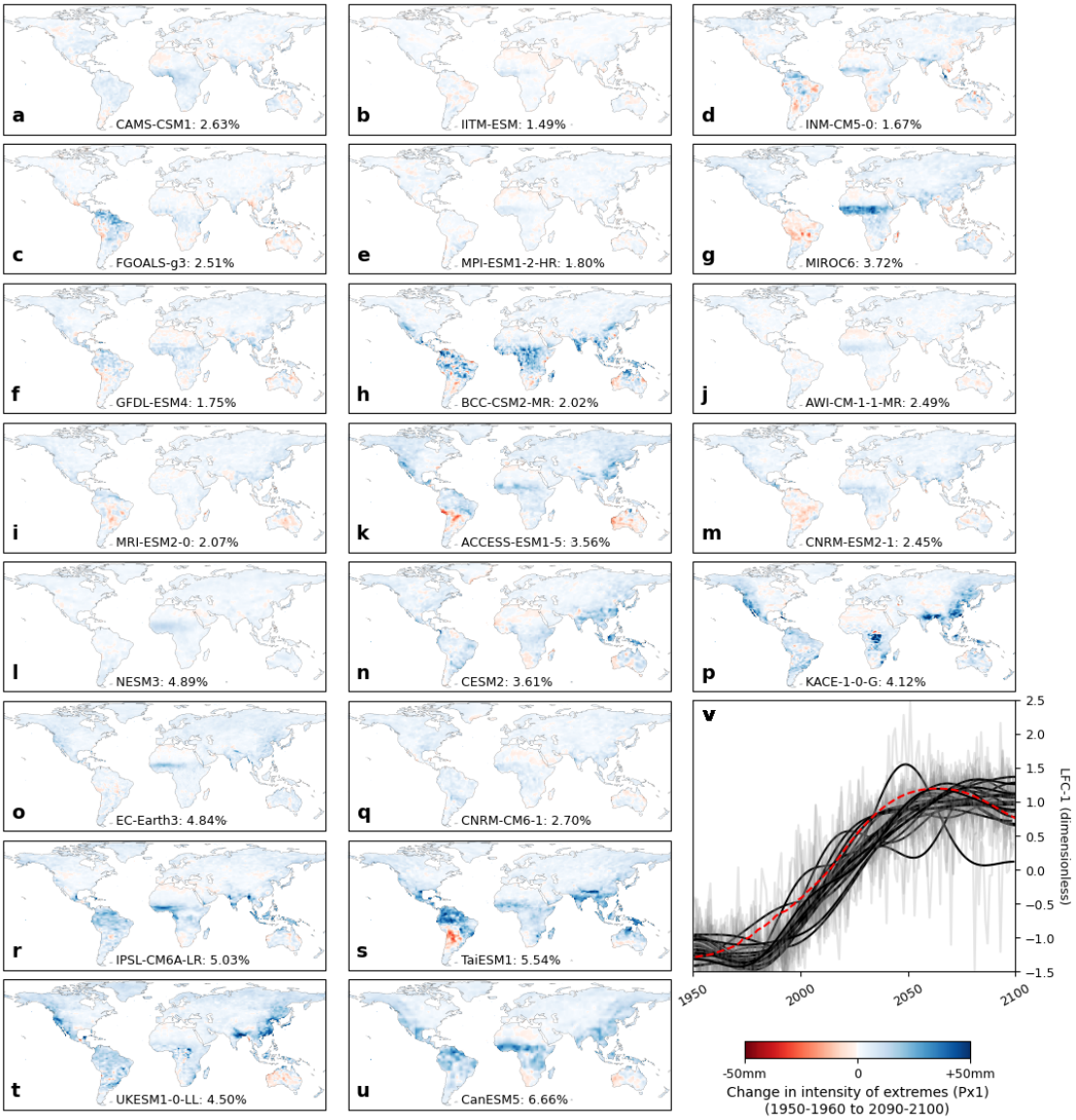

FIG. A6. As Fig. A5 but under the historical and SSP126 scenario greenhouse forcing.

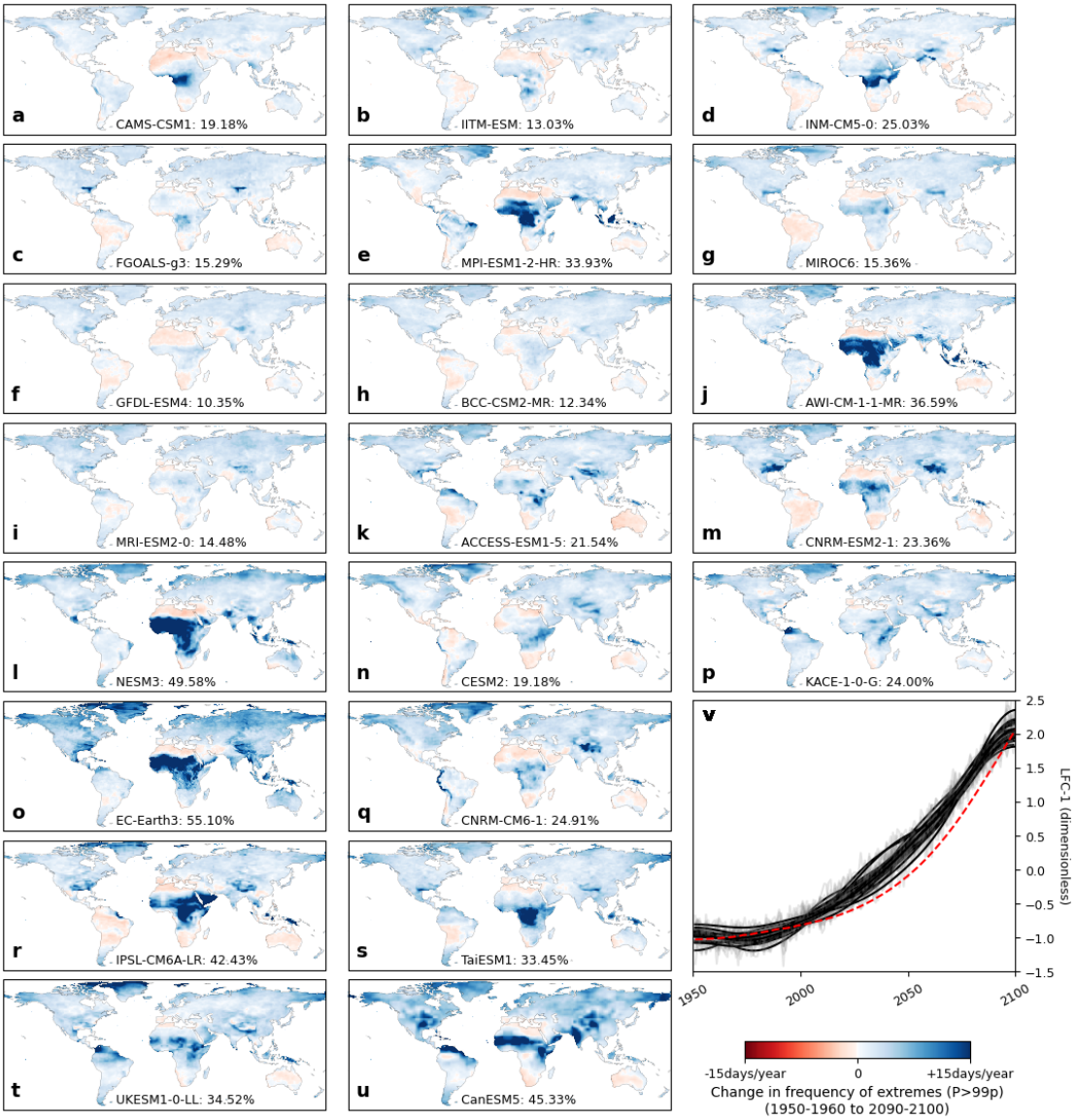

FIG. A7. The detected forced response of the frequency of daily extremes under historical and SSP585 scenario greenhouse forcing. As Fig. 1 but for all models in the CMIP6 ensemble. Models are ordered a-u in order of increasing GMT change.

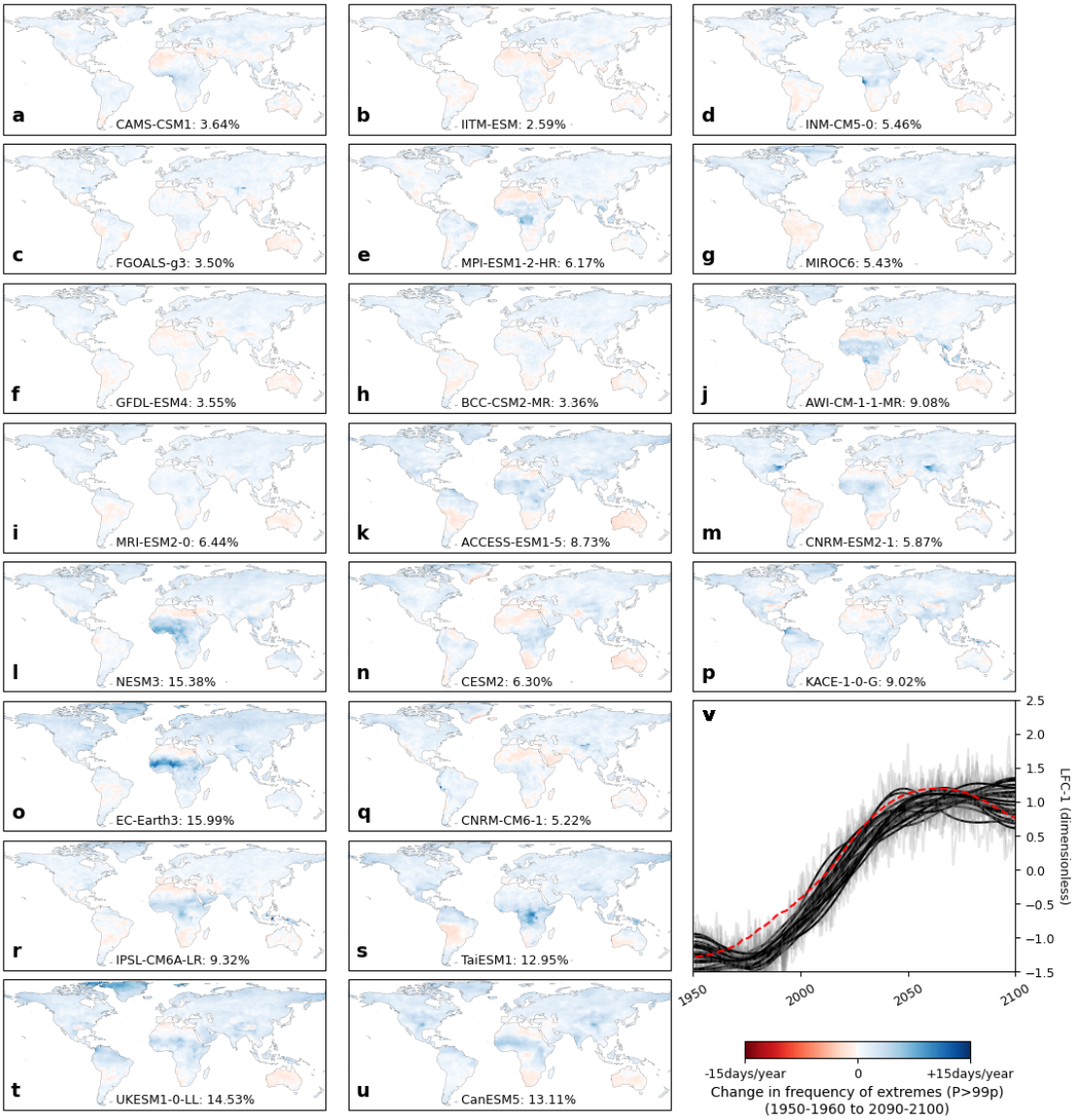

FIG. A8. As Fig. A7 but under the historical and SSP126 scenario greenhouse forcing.

APPENDIX B

Temperature-precipitation scaling

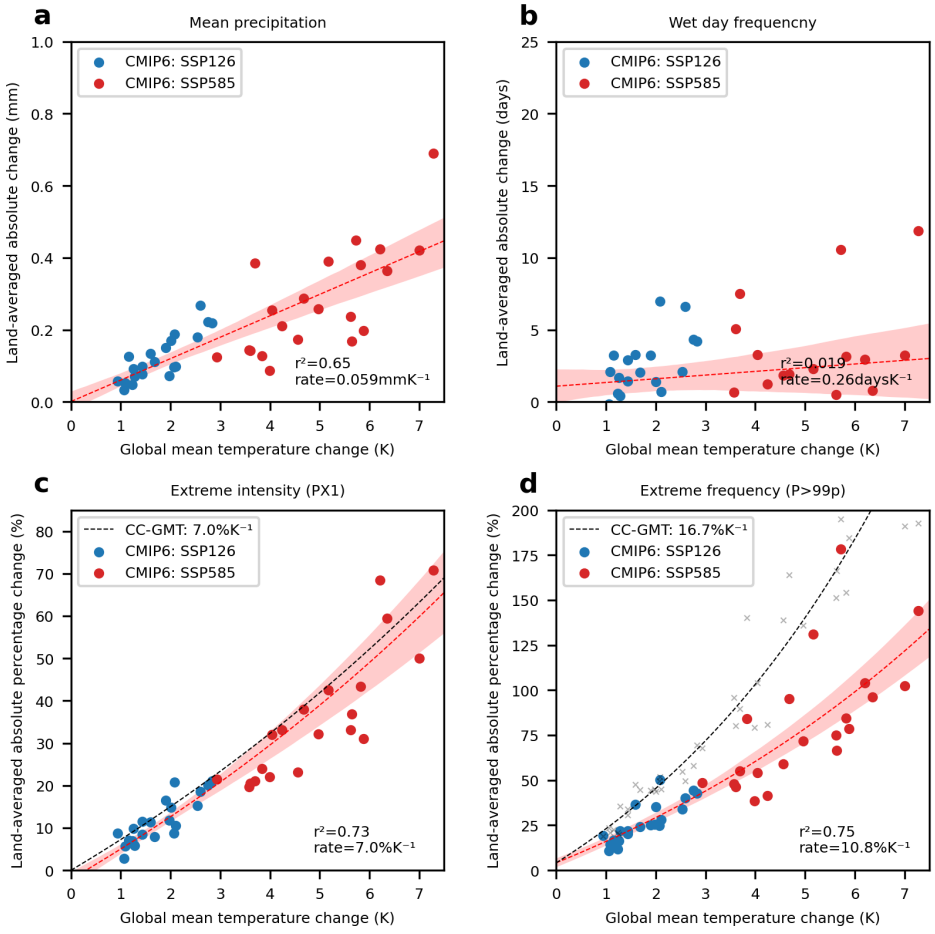

FIG. B1. Scaling between precipitation changes and GMT change without taking absolute values. As Fig. 4 but without taking absolute values of regional precipitation change.

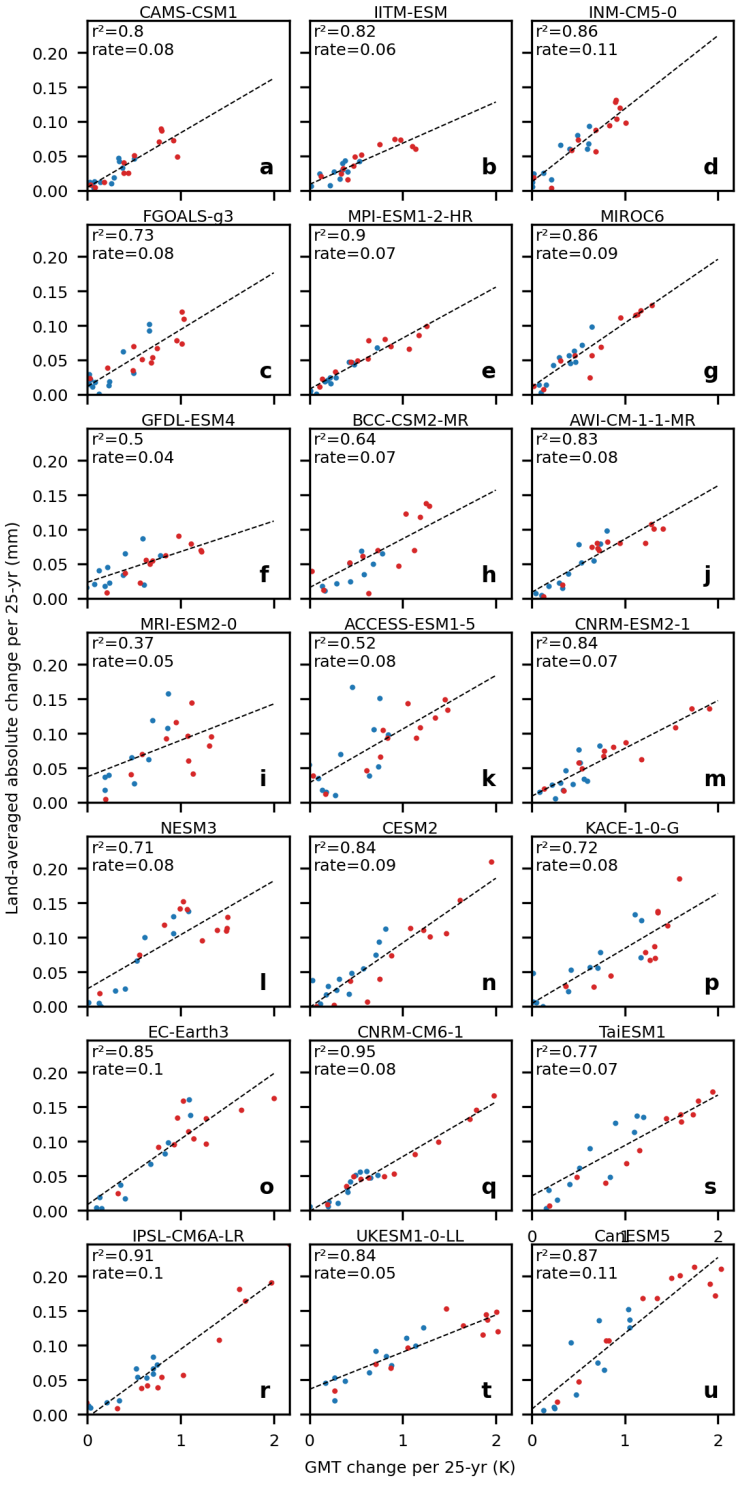

FIG. B2. Intra-model scaling between mean precipitation and GMT change for all members of the CMIP6 ensemble. As Fig. 5a-e but for all members.

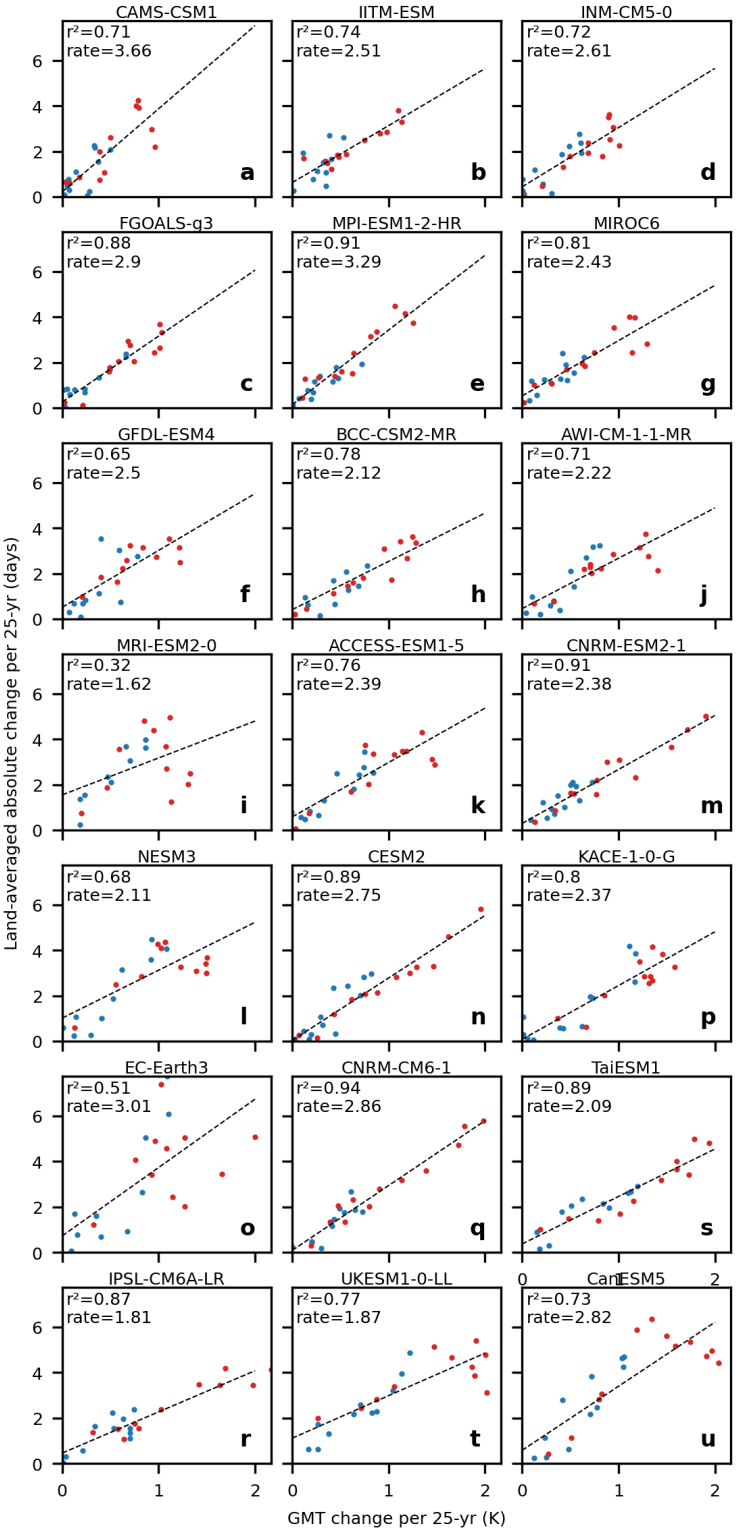

FIG. B3. Intra-model scaling between wet day frequency and GMT change for all members of the CMIP6 ensemble. As Fig. 5f-j but for all members.

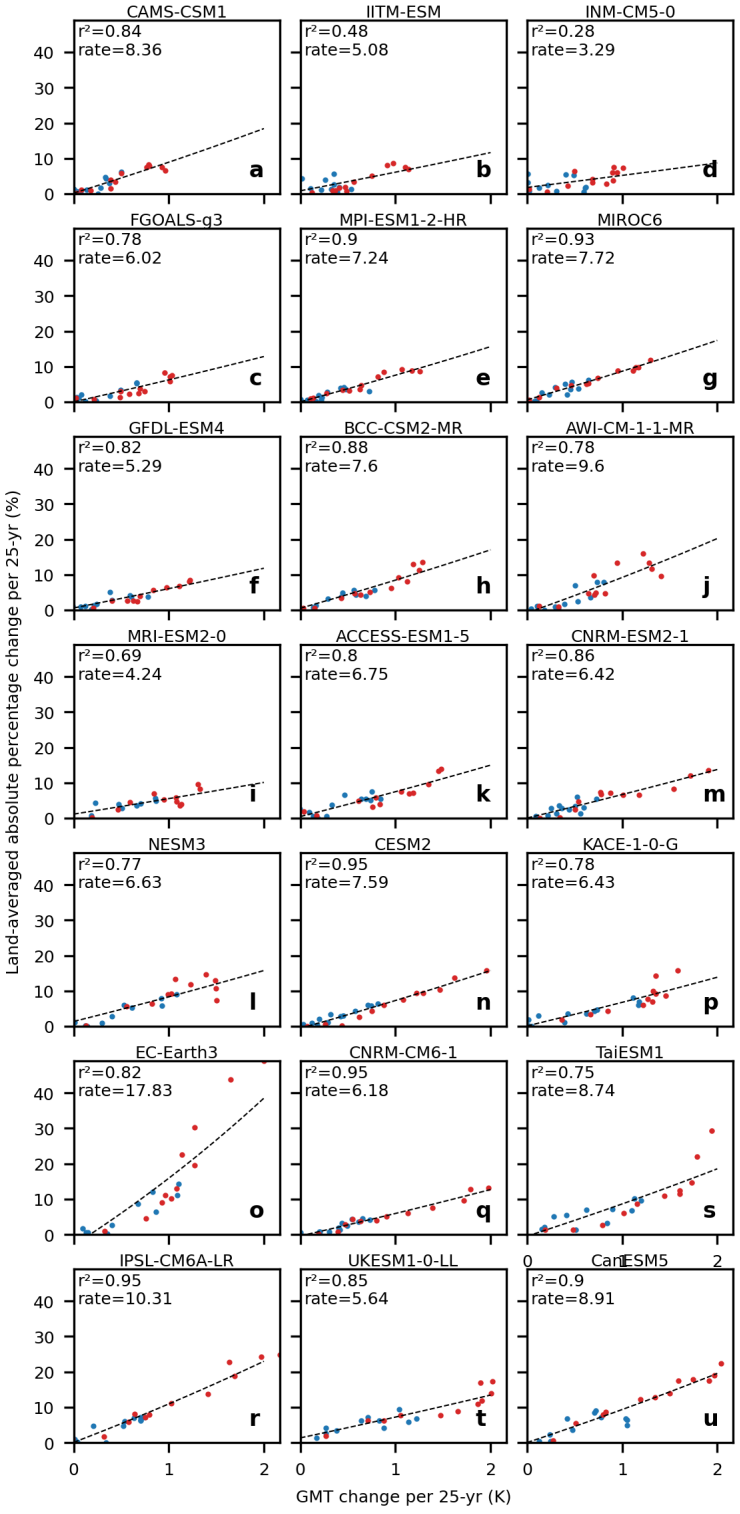

FIG. B4. Intra-model scaling between the intensity of daily extremes (PX1) and GMT change for all members of the CMIP6 ensemble. As Fig. 5k-o but for all members.

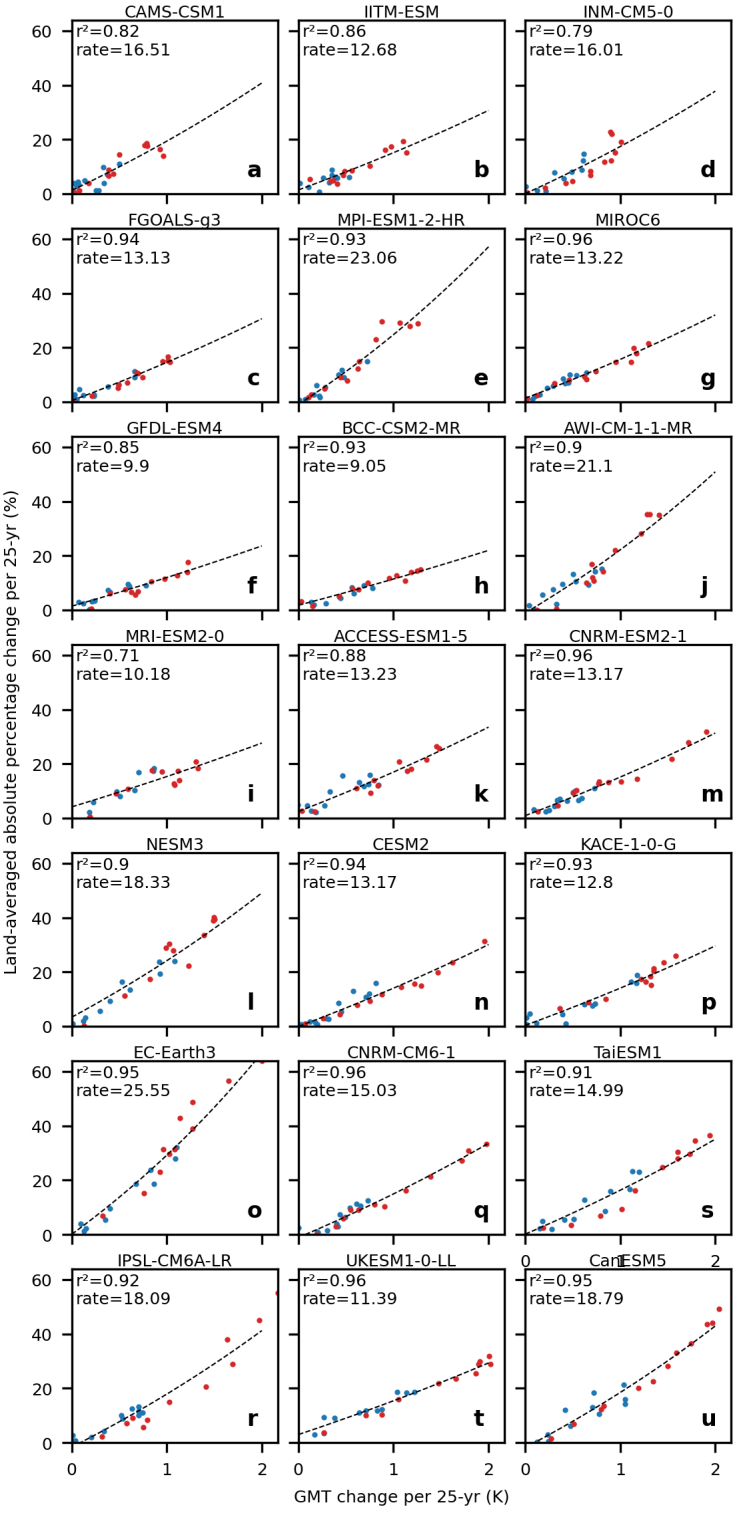

FIG. B5. Intra-model scaling between the frequency of daily extremes (P>99p) and GMT change for all members of the CMIP6 ensemble. As Fig. 5p-t but for all members.

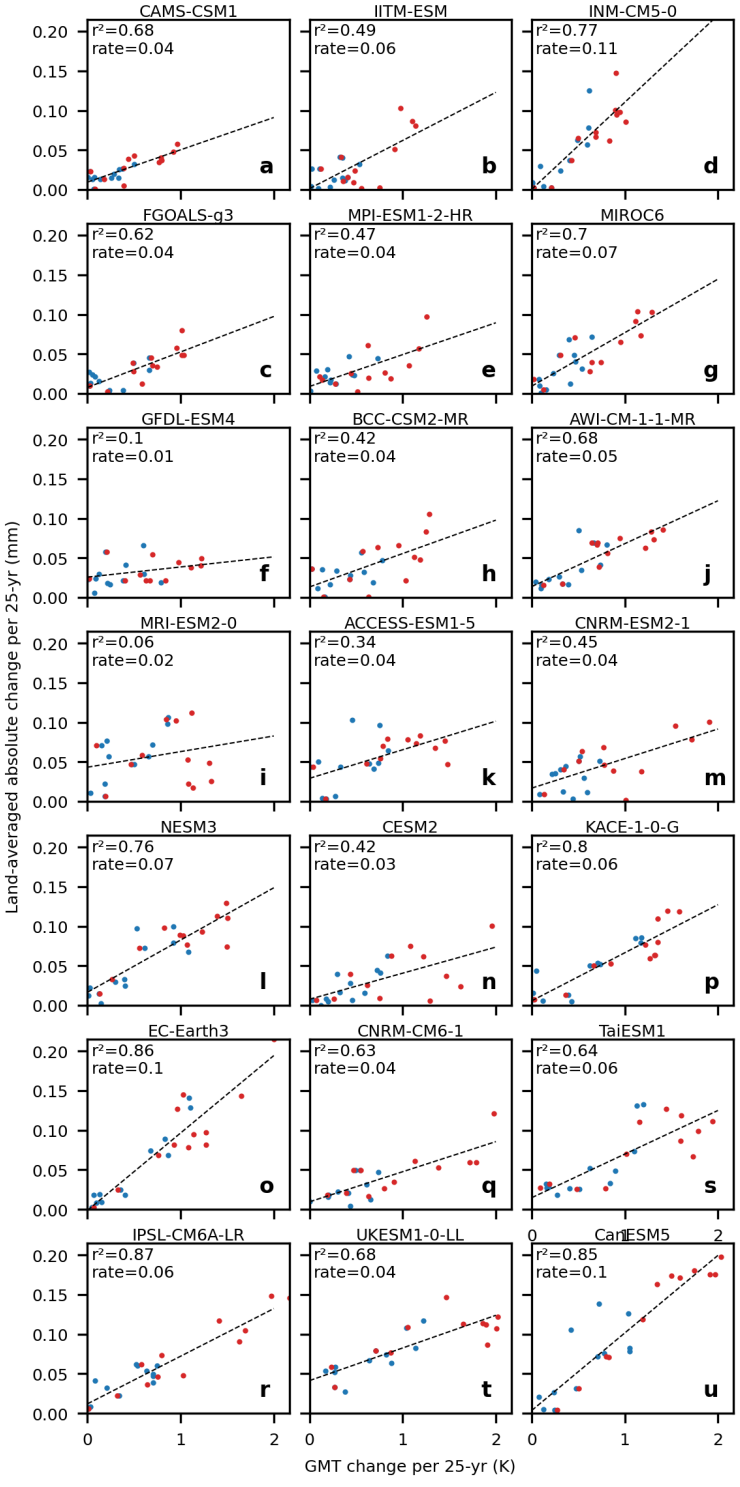

FIG. B6. As Fig. B2 but without having first applied LFCA.

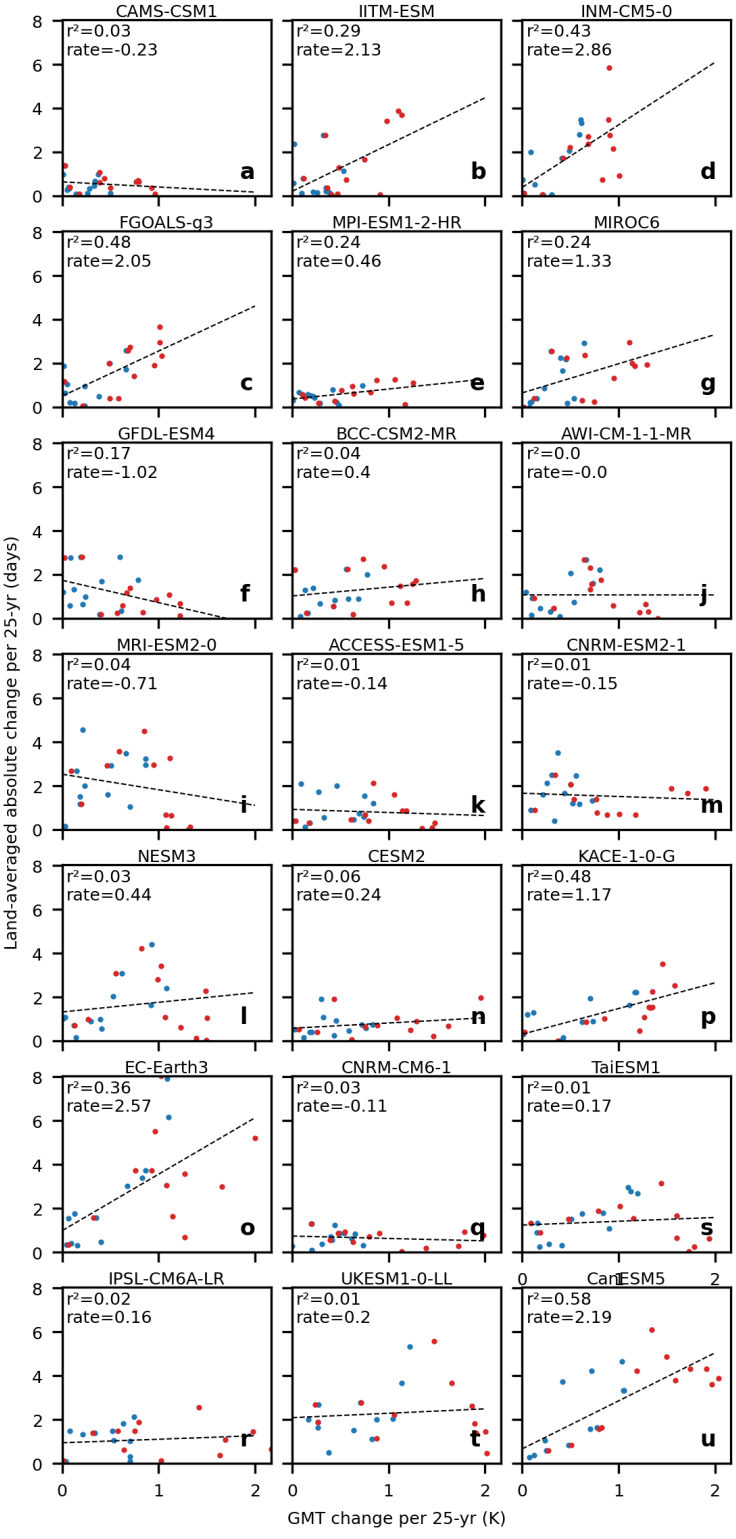

FIG. B7. As Fig. B3 but without having first applied LFCA.

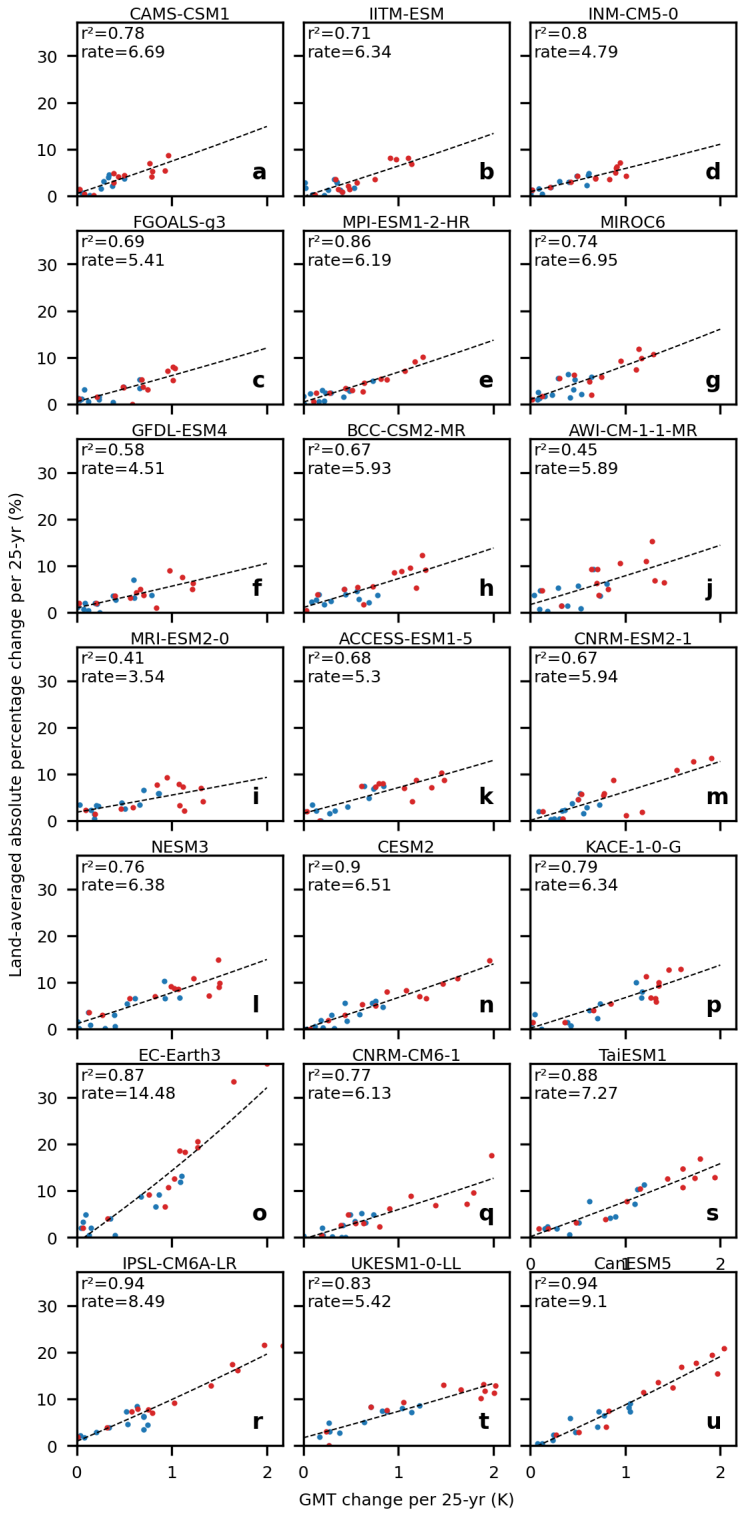

FIG. B8. As Fig. B4 but without having first applied LFCA.

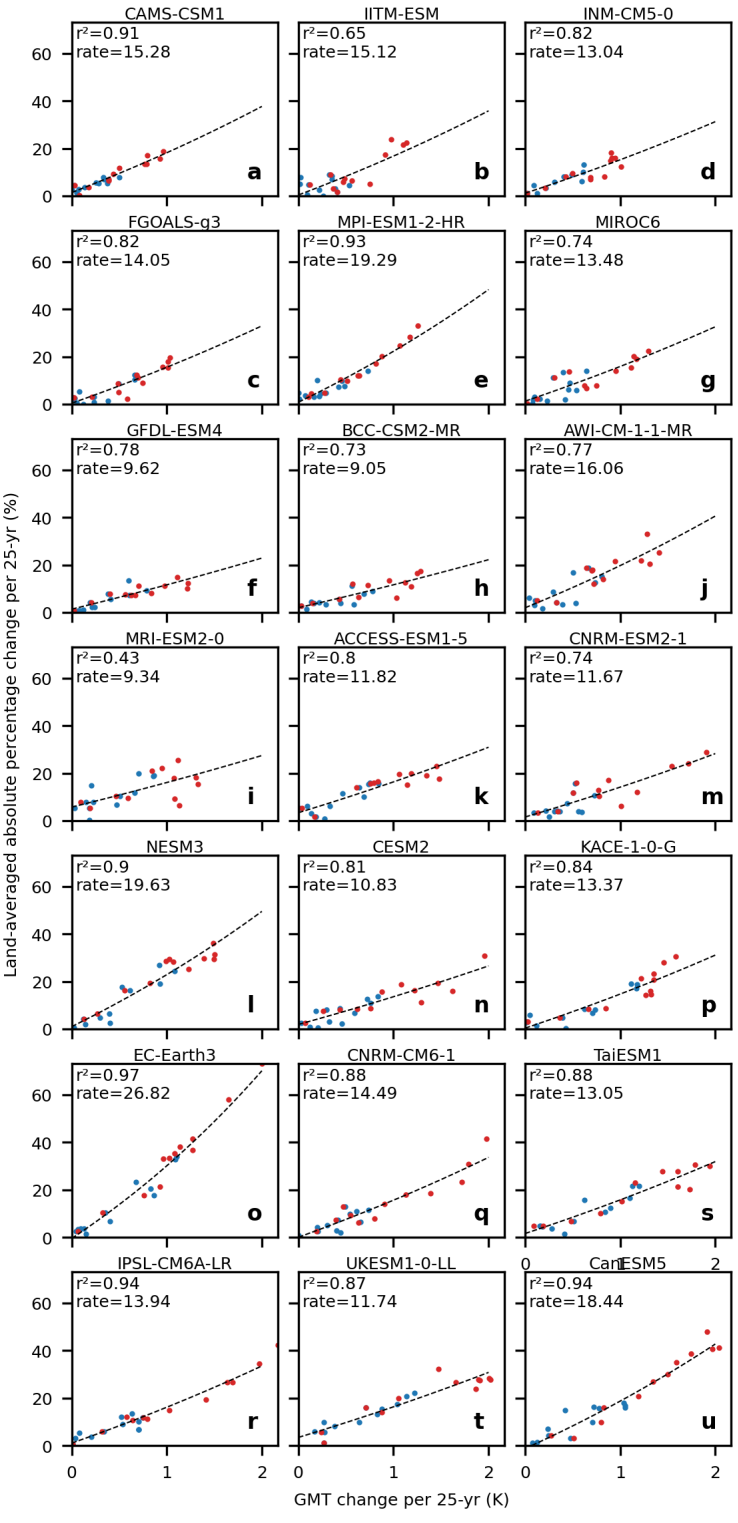

FIG. B9. As Fig. B5 but without having first applied LFCA.

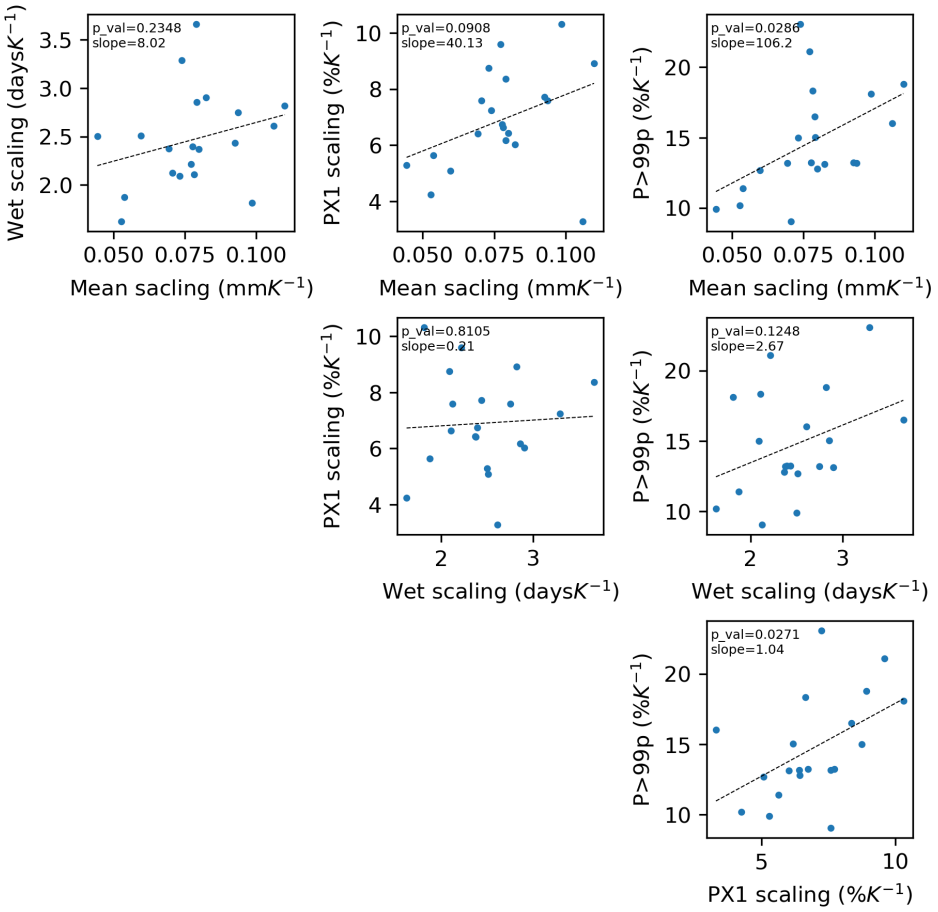

FIG. B10. Co-variation between models of the scaling rates of different precipitation characteristics. "Mean", "Wet", "PX1" and "P>99p" refer to the mean precipitation rate, the frequency of wet days, and the intensity and frequency of daily extremes respectively.

References

Allen, M. R., and W. J. Ingram, 2002: Constraints on future changes in climate and the hydrologic cycle. *Nature*, **419 (6903)**, 228–232.

Boulange, J., N. Hanasaki, D. Yamazaki, and Y. Pokhrel, 2021: Role of dams in reducing global flood exposure under climate change. *Nature Communications*, **12 (1)**, 417, https://doi.org/10.1038/s41467-020-20704-0, URL https://doi.org/10.1038/s41467-020-20704-0.

Chadwick, R., I. Boutle, and G. Martin, 2013: Spatial patterns of precipitation change in cmip5: Why the rich do not get richer in the tropics. *Journal of Climate*, **26 (11)**, 3803 – 3822, https://doi.org/10.1175/JCLI-D-12-00543.1, URL https://journals.ametsoc.org/view/journals/clim/26/11/jcli-d-12-00543.1.xml.

Chadwick, R., P. Good, T. Andrews, and G. Martin, 2014: Surface warming patterns drive tropical rainfall pattern responses to co2 forcing on all timescales. *Geophysical Research Letters*, **41 (2)**, 610–615, https://doi.org/https://doi.org/10.1002/2013GL058504, URL https://agupubs.onlinelibrary.wiley.com/doi/abs/10.1002/2013GL058504, https://agupubs.onlinelibrary.wiley.com/doi/pdf/10.1002/2013GL058504.

Chadwick, R., P. Good, G. Martin, and D. P. Rowell, 2016: Large rainfall changes consistently projected over substantial areas of tropical land. *Nature Climate Change*, **6 (2)**, 177–181, https://doi.org/10.1038/nclimate2805, URL https://doi.org/10.1038/nclimate2805.

Chen, H., and J. Sun, 2017: Contribution of human influence to increased daily precipitation extremes over china. *Geophysical Research Letters*, **44 (5)**, 2436–2444, https://doi.org/https://doi.org/10.1002/2016GL072439, URL https://agupubs.onlinelibrary.wiley.com/doi/abs/10.1002/2016GL072439, https://agupubs.onlinelibrary.wiley.com/doi/pdf/10.1002/2016GL072439.

Damania, R., S. Desbureaux, and E. Zaveri, 2020: Does rainfall matter for economic growth? evidence from global sub-national data (1990–2014). *Journal of Environmental Economics and Management*, **102**, 102 335, https://doi.org/https://doi.org/10.1016/j.jeem.2020.102335, URL https://www.sciencedirect.com/science/article/pii/S0095069620300589.

Davenport, F. V., M. Burke, and N. S. Diffenbaugh, 2021: Contribution of historical precipitation change to us flood damages. *Proceedings of the National Academy of Sciences*,

118 (4), https://doi.org/10.1073/pnas.2017524118, URL https://www.pnas.org/content/118/4/e2017524118, https://www.pnas.org/content/118/4/e2017524118.full.pdf.

Deser, C., A. Phillips, V. Bourdette, and H. Teng, 2012: Uncertainty in climate change projections: the role of internal variability. *Climate Dynamics*, **38 (3)**, 527–546, https://doi.org/10.1007/s00382-010-0977-x, URL https://doi.org/10.1007/s00382-010-0977-x.

Deser, C., and A. S. Phillips, 2009: Atmospheric circulation trends, 1950–2000: The relative roles of sea surface temperature forcing and direct atmospheric radiative forcing. *Journal of Climate*, **22 (2)**, 396 – 413, https://doi.org/10.1175/2008JCLI2453.1, URL https://journals.ametsoc.org/view/journals/clim/22/2/2008jcli2453.1.xml.

Deser, C., A. S. Phillips, M. A. Alexander, and B. V. Smoliak, 2014: Projecting north american climate over the next 50 years: Uncertainty due to internal variability. *Journal of Climate*, **27 (6)**, 2271 – 2296, https://doi.org/10.1175/JCLI-D-13-00451.1, URL https://journals.ametsoc.org/view/journals/clim/27/6/jcli-d-13-00451.1.xml.

Eyring, V., S. Bony, G. A. Meehl, C. A. Senior, B. Stevens, R. J. Stouffer, and K. E. Taylor, 2016: Overview of the coupled model intercomparison project phase 6 (cmip6) experimental design and organization. *Geoscientific Model Development*, **9 (5)**, 1937–1958, https://doi.org/10.5194/gmd-9-1937-2016, URL https://gmd.copernicus.org/articles/9/1937/2016/.

Fereday, D., R. Chadwick, J. Knight, and A. A. Scaife, 2018: Atmospheric dynamics is the largest source of uncertainty in future winter european rainfall. *Journal of Climate*, **31 (3)**, 963 – 977, https://doi.org/10.1175/JCLI-D-17-0048.1, URL https://journals.ametsoc.org/view/journals/clim/31/3/jcli-d-17-0048.1.xml.

Fischer, E. M., and R. Knutti, 2016: Observed heavy precipitation increase confirms theory and early models. *Nature Climate Change*, **6 (11)**, 986–991, https://doi.org/10.1038/nclimate3110, URL https://doi.org/10.1038/nclimate3110.

Held, I. M., and B. J. Soden, 2006: Robust responses of the hydrological cycle to global warming. *Journal of climate*, **19 (21)**, 5686–5699.

Herger, N., B. M. Sanderson, and R. Knutti, 2015: Improved pattern scaling approaches for the use in climate impact studies. *Geophysical Research Letters*, **42 (9)**, 3486–3494.

Holtermann, L., 2020: Precipitation anomalies, economic production, and the role of "first-nature" and "second-nature" geographies: A disaggregated analysis in high-income countries. *Global Environmental Change*, **65**, 102 167, https://doi.org/https://doi.org/10.1016/j.gloenvcha.2020.102167, URL https://www.sciencedirect.com/science/article/pii/S0959378020307500.

Hsiang, S. M., M. Burke, and E. Miguel, 2013: Quantifying the influence of climate on human conflict. *Science*, **341 (6151)**, 1235 367, https://doi.org/10.1126/science.1235367.

Kay, J. E., and Coauthors, 2015: The community earth system model (cesm) large ensemble project: A community resource for studying climate change in the presence of internal climate variability. *Bulletin of the American Meteorological Society*, **96 (8)**, 1333 – 1349, https://doi.org/10.1175/BAMS-D-13-00255.1, URL https://journals.ametsoc.org/view/journals/bams/96/8/bams-d-13-00255.1.xml.

Kent, C., R. Chadwick, and D. P. Rowell, 2015: Understanding uncertainties in future projections of seasonal tropical precipitation. *Journal of Climate*, **28 (11)**, 4390 – 4413, https://doi.org/10.1175/JCLI-D-14-00613.1, URL https://journals.ametsoc.org/view/journals/clim/28/11/jcli-d-14-00613.1.xml.

Kirchmeier-Young, M. C., and X. Zhang, 2020: Human influence has intensified extreme precipitation in north america. *Proceedings of the National Academy of Sciences*, **117 (24)**, 13 308–13 313, https://doi.org/10.1073/pnas.1921628117, URL https://www.pnas.org/content/117/24/13308, https://www.pnas.org/content/117/24/13308.full.pdf.

Knutti, R., and J. Sedláček, 2013: Robustness and uncertainties in the new cmip5 climate model projections. *Nature climate change*, **3 (4)**, 369–373.

Kotz, M., A. Levermann, and L. Wenz, 2022: The effect of rainfall changes on economic production. *Nature*, https://doi.org/10.1038/s41586-021-04283-8.

Kotz, M., L. Wenz, and A. Levermann, 2021: Footprint of greenhouse forcing in daily temperature variability. *Proceedings of the National Academy of Sciences*, **118 (32)**, https://doi.org/10.1073/pnas.2103294118, URL https://www.pnas.org/content/118/32/e2103294118, https://www.pnas.org/content/118/32/e2103294118.full.pdf.

Lange, S., and Coauthors, 2020: Projecting exposure to extreme climate impact events across six event categories and three spatial scales. *Earth's Future*, **8 (12)**, e2020EF001 616, https://doi.org/ https://doi.org/10.1029/2020EF001616, URL https://agupubs.onlinelibrary.wiley.com/doi/ abs/10.1029/2020EF001616, e2020EF001616 10.1029/2020EF001616, https://agupubs. onlinelibrary.wiley.com/doi/pdf/10.1029/2020EF001616.

Liang, X.-Z., and Coauthors, 2017: Determining climate effects on us total agricultural productivity. *Proceedings of the National Academy of Sciences*, **114 (12)**, E2285–E2292, https://doi.org/10.1073/pnas.1615922114, URL https://www.pnas.org/content/114/12/E2285, https://www.pnas.org/content/114/12/E2285.full.pdf.

Long, S.-M., S.-P. Xie, and W. Liu, 2016: Uncertainty in tropical rainfall projections: Atmospheric circulation effect and the ocean coupling. *Journal of Climate*, **29 (7)**, 2671 – 2687, https://doi.org/10.1175/JCLI-D-15-0601.1, URL https://journals.ametsoc.org/view/ journals/clim/29/7/jcli-d-15-0601.1.xml.

Ma, J., and S.-P. Xie, 2013: Regional patterns of sea surface temperature change: A source of uncertainty in future projections of precipitation and atmospheric circulation. *Journal of Climate*, **26 (8)**, 2482 – 2501, https://doi.org/10.1175/JCLI-D-12-00283.1, URL https://journals.ametsoc. org/view/journals/clim/26/8/jcli-d-12-00283.1.xml.

Madakumbura, G., C. C.W. Thackeray, and J. J. Norris, 2021: Anthropogenic influence on extreme precipitation over global land areas seen in multiple observational datasets. *Nature Communications*, **12 (3944)**, https://doi.org/10.1073/pnas.1921628117.

Marvel, K., and C. Bonfils, 2013: Identifying external influences on global precipitation. *Proceedings of the National Academy of Sciences*, **110 (48)**, 19 301–19 306, https://doi.org/10.1073/pnas. 1314382110, URL https://www.pnas.org/content/110/48/19301, https://www.pnas.org/content/ 110/48/19301.full.pdf.

Masson-Delmotte, V., and Coauthors, 2021: IPCC, 2021: Climate Change 2021: The Physical Science Basis. Contribution of Working Group I to the Sixth Assessment Report of the Intergovernmental Panel on Climate Change. *Cambridge University Press. In Press.*

Min, S.-K., X. Zhang, F. W. Zwiers, and G. C. Hegerl, 2011: Human contribution to more-intense precipitation extremes. *Nature*, **470 (7334)**, 378–381, https://doi.org/10.1038/nature09763, URL https://doi.org/10.1038/nature09763.

Myhre, G., and Coauthors, 2019: Frequency of extreme precipitation increases extensively with event rareness under global warming. *Scientific Reports*, **9 (1)**, 16 063, https://doi.org/10.1038/s41598-019-52277-4, URL https://doi.org/10.1038/s41598-019-52277-4.

O'Gorman, P. A., 2012: Sensitivity of tropical precipitation extremes to climate change. *Nature Geoscience*, **5 (10)**, 697–700, https://doi.org/10.1038/ngeo1568, URL https://doi.org/10.1038/ngeo1568.

Pfahl, S., P. A. O'Gorman, and E. M. Fischer, 2017: Understanding the regional pattern of projected future changes in extreme precipitation. *Nature Climate Change*, **7 (6)**, 423–427, https://doi.org/10.1038/nclimate3287, URL https://doi.org/10.1038/nclimate3287.

Schewe, J., and A. Levermann, 2022: Sahel rainfall projections constrained by past sensitivity to global warming. *Geophysical Research Letters*, e2022GL098286.

Shepherd, T. G., 2014: Atmospheric circulation as a source of uncertainty in climate change projections. *Nature Geoscience*, **7 (10)**, 703–708, https://doi.org/10.1038/ngeo2253, URL https://doi.org/10.1038/ngeo2253.

Shiogama, H., M. Watanabe, H. Kim, and N. Hirota, 2022: Emergent constraints on future precipitation changes. *Nature*, **602 (7898)**, 612–616.

Thiery, W., and Coauthors, 2021: Intergenerational inequities in exposure to climate extremes. *Science*, **374 (6564)**, 158–160, https://doi.org/10.1126/science.abi7339.

Vecchi, G. A., and B. J. Soden, 2007: Global warming and the weakening of the tropical circulation. *Journal of Climate*, **20 (17)**, 4316–4340.

Vecchi, G. A., B. J. Soden, A. T. Wittenberg, I. M. Held, A. Leetmaa, and M. J. Harrison, 2006: Weakening of tropical pacific atmospheric circulation due to anthropogenic forcing. *Nature*, **441 (7089)**, 73–76.

von Uexkull, N., M. Croicu, H. Fjelde, and H. Buhaug, 2016: Civil conflict sensitivity to growing-season drought. *Proceedings of the National Academy of Sciences*, **113 (44)**, 12 391–12 396, https://doi.org/10.1073/pnas.1607542113, URL https://www.pnas.org/content/113/44/12391, https://www.pnas.org/content/113/44/12391.full.pdf.

Warszawski, L., K. Frieler, V. Huber, F. Piontek, O. Serdeczny, and J. Schewe, 2014: The inter-sectoral impact model intercomparison project (isi–mip): Project framework. *Proceedings of the National Academy of Sciences*, **111 (9)**, 3228–3232, https://doi.org/10.1073/pnas.1312330110, URL https://www.pnas.org/content/111/9/3228, https://www.pnas.org/content/111/9/3228.full.pdf.

Williamson, M. S., C. W. Thackeray, P. M. Cox, A. Hall, C. Huntingford, and F. J. Nijsse, 2021: Emergent constraints on climate sensitivities. *Reviews of Modern Physics*, **93 (2)**, 025 004.

Willner, S. N., A. Levermann, F. Zhao, and K. Frieler, 2018a: Adaptation required to preserve future high-end river flood risk at present levels. *Science Advances*, **4 (1)**, eaao1914, https://doi.org/10.1126/sciadv.aao1914.

Willner, S. N., C. Otto, and A. Levermann, 2018b: Global economic response to river floods. *Nature Climate Change*, **8 (7)**, 594–598, https://doi.org/10.1038/s41558-018-0173-2, URL https://doi.org/10.1038/s41558-018-0173-2.

Wills, R. C., T. Schneider, J. M. Wallace, D. S. Battisti, and D. L. Hartmann, 2018: Disentangling global warming, multidecadal variability, and el niño in pacific temperatures. *Geophysical Research Letters*, **45 (5)**, 2487–2496, https://doi.org/https://doi.org/10.1002/2017GL076327, URL https://agupubs.onlinelibrary.wiley.com/doi/abs/10.1002/2017GL076327, https://agupubs.onlinelibrary.wiley.com/doi/pdf/10.1002/2017GL076327.

Wills, R. C. J., D. S. Battisti, K. C. Armour, T. Schneider, and C. Deser, 2020: Pattern recognition methods to separate forced responses from internal variability in climate model ensembles and observations. *Journal of Climate*, **33 (20)**, 8693 – 8719, https://doi.org/10.1175/JCLI-D-19-0855.1, URL https://journals.ametsoc.org/view/journals/clim/33/20/jcliD190855.xml.

Zhang, X., H. Wan, F. W. Zwiers, G. C. Hegerl, and S.-K. Min, 2013: Attributing intensification of precipitation extremes to human influence. *Geophysical Research Letters*, **40 (19)**, 5252–5257, https://doi.org/https://doi.org/10.1002/grl.51010, URL https://agupubs.onlinelibrary.wiley.com/doi/abs/10.1002/grl.51010, https://agupubs.onlinelibrary.wiley.com/doi/pdf/10.1002/grl.51010.